Stem Cell Reports
Article

ISSCR

OPEN ACCESS

Direct Reprogramming of Human Bone Marrow Stromal Cells into Functional Renal Cells Using Cell-free Extracts

Evangelia Papadimou,[1,*] Marina Morigi,[1] Paraskevas Iatropoulos,[2] Christodoulos Xinaris,[1] Susanna Tomasoni,[1] Valentina Benedetti,[1] Lorena Longaretti,[1] Cinzia Rota,[1] Marta Todeschini,[2] Paola Rizzo,[1] Martino Introna,[3] Maria Grazia de Simoni,[4] Giuseppe Remuzzi,[1,2,5,*] Michael S. Goligorsky,[6,7] and Ariela Benigni[1,7]

[1]IRCCS-Istituto di Ricerche Farmacologiche "Mario Negri," Centro Anna Maria Astori, Science and Technology Park Kilometro Rosso, 24126 Bergamo, Italy
[2]IRCCS-Istituto di Ricerche Farmacologiche "Mario Negri," Clinical Research Center for Rare Diseases "Aldo e Cele Daccò," 24020 Ranica, Italy
[3]Laboratory of Cellular Therapy "G. Lanzani," USC Hematology, 24122 Bergamo, Italy
[4]Department of Neuroscience, IRCCS - Istituto di Ricerche Farmacologiche "Mario Negri," 20156 Milan, Italy
[5]Unit of Nephrology and Dialysis, Azienda Ospedaliera Papa Giovanni XXIII, 24127 Bergamo, Italy
[6]Department of Medicine, Renal Research Institute, New York Medical College, 15 Dana Road, BSB C-06, Valhalla, NY 10595, USA
[7]Co-senior author
*Correspondence: evangelia.papadimou@marionegri.it (E.P.), giuseppe.remuzzi@marionegri.it (G.R.)
http://dx.doi.org/10.1016/j.stemcr.2015.02.002

SUMMARY

The application of cell-based therapies in regenerative medicine is gaining recognition. Here, we show that human bone marrow stromal cells (BMSCs), also known as bone-marrow-derived mesenchymal cells, can be reprogrammed into renal proximal tubular-like epithelial cells using cell-free extracts. Streptolysin-O-permeabilized BMSCs exposed to HK2-cell extracts underwent morphological changes—formation of "domes" and tubule-like structures—and acquired epithelial functional properties such as transepithelial-resistance, albumin-binding, and uptake and specific markers E-cadherin and aquaporin-1. Transmission electron microscopy revealed the presence of brush border microvilli and tight intercellular contacts. RNA sequencing showed tubular epithelial transcript abundance and revealed the up-regulation of components of the *EGFR* pathway. Reprogrammed BMSCs integrated into self-forming kidney tissue and formed tubular structures. Reprogrammed BMSCs infused in immunodeficient mice with cisplatin-induced acute kidney injury engrafted into proximal tubuli, reduced renal injury and improved function. Thus, reprogrammed BMSCs are a promising cell resource for future cell therapy.

INTRODUCTION

Cell-based therapies are emerging as one of the most promising approaches of regenerative medicine (Riazi et al., 2009). In the kidney field, the search for a renal-specific stem cell led to the discovery of progenitor cells that protect animals from acute kidney injury (AKI) when systemically infused (Angelotti et al., 2012; Benigni et al., 2010). However, the cell number is a limiting factor, and their biology is far from known. Therefore, other non-renal stem cell sources have been pursued. Derivation of human embryonic stem cells (hESCs) (Thomson et al., 1998) has raised hope because they can give rise to all three germ layers, but progress toward somatic populations has encountered major obstacles, including the risk of cancer and rejection, not to mention the ethical issues involved. The same holds true for induced pluripotent stem cells (iPSCs) (Takahashi and Yamanaka, 2006), which are similar to hESCs but devoid of at least some of the above problems. The generation of hESC/iPSC-derived mature renal cells (Song et al., 2012) and, more recently, intermediate mesoderm/metanephric mesenchyme (MM) and ureteric bud (UB) renal progenitors (Lam et al., 2014; Lin et al., 2010; Mae et al., 2013; Takasato et al., 2014) has been reported. In principle, patient-specific cells to be used therapeutically could be obtained through reprogramming approaches in which a long-standing interest exists because of the possibility that abundant adult cells can easily be harvested and converted to other cell types (Zhou et al., 2008). In this context, studies have defined sets of transcription factors that can directly reprogram somatic cells into another cell type without passing through the pluripotent state (Ginsberg et al., 2012; Ieda et al., 2010; Karow et al., 2012; Vierbuchen et al., 2010). Using a strategy of re-expressing key developmental regulators in vitro/in vivo, adult cell reprogramming occurs, through which induced cells residing in their native environment might promote their survival and/or maturation (Ginsberg et al., 2012; Ieda et al., 2010; Karow et al., 2012; Qian et al., 2012; Vierbuchen et al., 2010; Zhou et al., 2008).

In parallel with these developments, an intriguing technology for direct cell reprogramming by exposing reversibly permeabilized somatic cells to cell-free extracts has emerged. This method has its origins in the early experiments of Briggs and King, followed by Gurdon (Gurdon, 2006), where a somatic cell nucleus was transferred (SCNT [somatic cell nuclear transfer]) to an enucleated oocyte, resulting in the activation of the somatic cell

nucleus. Cell-extract reprogramming was first demonstrated with extracts of regenerating newt limbs, which promoted cell-cycle re-entry and downregulation of myogenic markers in differentiated myotubes (McGann et al., 2001). Afterward, this approach yielded in-vitro-reprogrammed somatic cells with the extracts from T cells, cardiomyocytes, insulinoma cells, pneumocytes, chromaffin, or embryonic stem cells (Gaustad et al., 2004; Håkelien et al., 2002, 2004; Landsverk et al., 2002; Qin et al., 2005; Qu et al., 2013; Rajasingh et al., 2008).

Surprisingly, there is a paucity of attempts at the reverse reprogramming of adult stem cells toward somatic cells. Human bone marrow stromal cells (BMSCs), also known as bone-marrow-derived mesenchymal stem cells, are adult stem/progenitor cells with self-renewal capacity and restricted potential for generating skeletal tissues, including osteoblast, chondrocyte, adipocyte, and perivascular stromal cells (Bianco et al., 2013; Le Blanc and Mougiakakos, 2012). Whether BMSCs can be used therapeutically is still a matter of debate. Based on their paracrine action rather than differentiation ability, these cells have been used with promising results in different diseases (Le Blanc and Mougiakakos, 2012; Morigi and Benigni, 2013; Reinders et al., 2014; Souidi et al., 2013). No evidence of direct reprogramming of BMSCs into somatic cells is available yet.

Here, we inquired whether human BMSCs could be reverse reprogrammed to acquire a renal tubular epithelial phenotype by using tubular cell extracts. We found that reprogrammed BMSCs (1) acquired an antigenic profile and functional properties of proximal tubular-like epithelial cells in vitro, (2) integrated into developing nephrons ex vivo, and (3) protected mice from AKI.

RESULTS

Morphological and Ultrastructural Characteristics of BMSCs Treated with HK2 Cell Extracts

Human BMSCs were permeabilized with 400 ng/ml streptolysin O (SLO), a concentration that did not affect cell viability. Permeabilized BMSCs exposed to the extract of human proximal tubular epithelial (HK2) cells changed from their usual spindle-shape appearance (Figure 1A) to cobblestone islands within 13–15 days (Figures 1B–1D). During the subsequent 2 weeks, these islands expanded and the formation of "domes" and tubular-like structures (Figures 1E and 1F) similar to HK2 cells (Figure 1H) occurred. This morphological transition did not occur in BMSCs grown in epithelial-specific culture medium, even after 35 days (Figures 1I and 1J). The observed change in morphological appearance of BMSCs treated with epithelial cell extract suggested a phenotypic switch in the cells.

Moreover, transmission electron microscopy (TEM) of cell-extract-treated BMSCs demonstrated brush border microvilli and images of tight intercellular contact (Figures 1K–1M), further confirming that cells acquired a proximal tubular-like epithelial phenotype similar to HK2 cells (Figures 1N and 1O). BMSCs treated with HK2 cell medium did not demonstrate any apical specialization or cell-cell contact, even after 35 days (Figure 1P).

Antigenic Profile of the BMSCs Treated with HK2 Cell Extracts

To explore the renal identity of BMSCs treated with HK2 cell extracts, we studied candidate proximal tubular epithelial cell markers using immunofluorescence microscopy and flow cytometry (fluorescence-activated cell sorting [FACS]) analysis. BMSCs consistently expressed endoglin (ENG; also known as CD105), characteristic of the mesenchymal lineage, and were devoid of the epithelial markers E-cadherin (CDH1) and aquaporin-1 (AQP1) (Figures S1A–S1D). After 8 days, BMSCs treated with HK2 cell extracts weakly expressed CDH1, TJP1 (tight junction protein 1; also known as zona occludens-1), and AQP1 in combination with BMSC markers (Figures 2A–2D). Moreover, after 25 days, BMSCs treated with HK2 cell extracts displayed robust expression of the epithelial markers but substantially reduced expression of ENG (Figures 2E and 2H), which is consistent with the expression profile of HK2 cells (Figures S1E–S1H). Notably, BMSCs that were not converted to cobblestone islands maintained the expression of mesenchymal markers (Figures 2E and 2H, area defined by the dotted line). BMSCs grown in HK2 cell medium, used as control, did not express epithelial markers and retained the expression of ENG (Figures S1I–S1L).

To quantify the BMSC reprogramming process, FACS analysis was performed. By day 8, a cell population of 1%–3% of BMSCs treated with HK2 cell extracts expressed AQP1 and CDH1 (Figure 2I). The highest percentage of reprogrammed BMSCs expressing these tubular epithelial markers was observed after 35 days and averaged 15%–21% (Figure 2I).

To trace the reprogramming process chronologically, we used an EGFP plasmid containing the promoter region of *CDH1* (Genecopeia; HPRM12692-PF02). Human BMSCs were transfected at days 5 and 11 from cell-extract exposure, and CDH1/EGFP-positive cells were assessed 24 hr later (days 6 and 12). At day 6, the EGFP-positive cells had a BMSC-like shape, while at day 12, CDH1/EGFP-positive cells acquired an epithelial-like appearance (Figure 2J). The reprogramming efficiency was ~0.01%–0.02%. Untreated BMSCs grown in HK2 cell medium did not express EGFP at any time points tested (Figure 2J). As expected, several HK2-transfected cells became positive for CDH1/EGFP, with a transfection efficiency of 30% (Figure 2J).

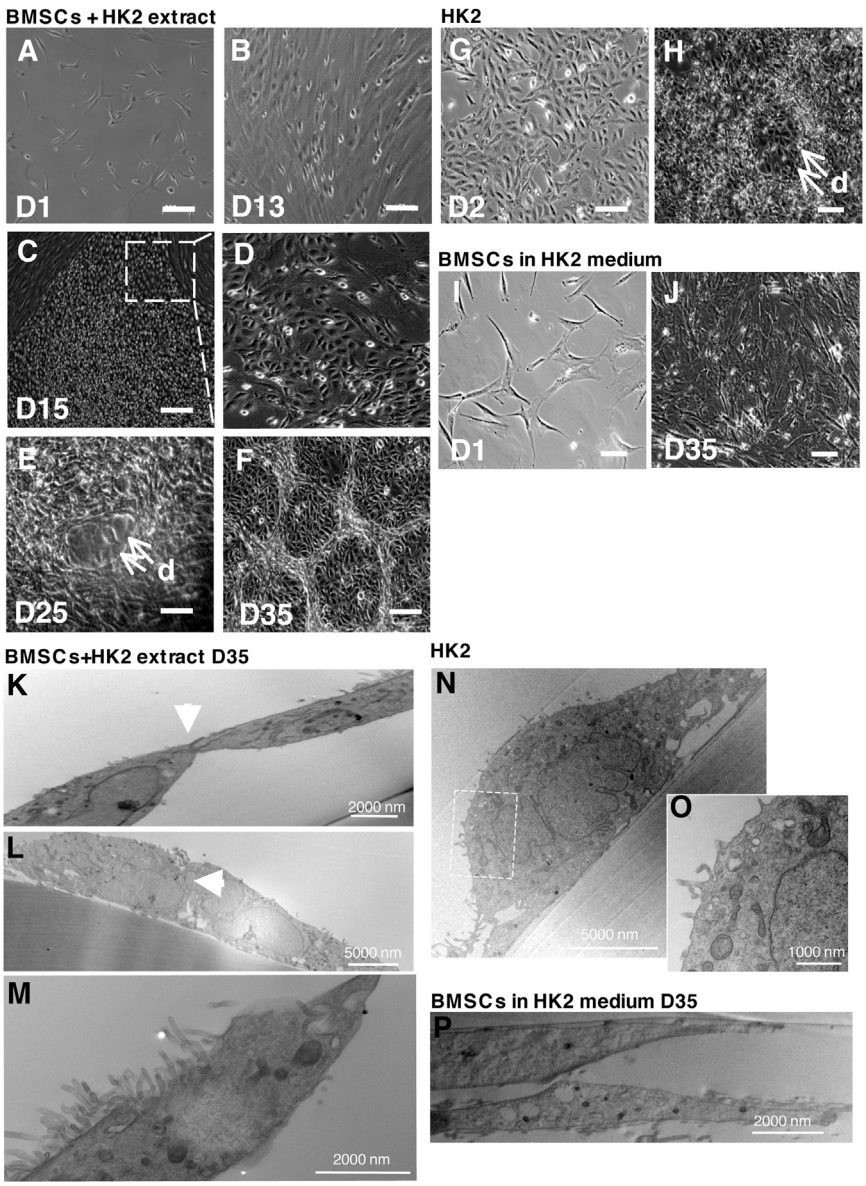

Figure 1. Morphological and Ultrastructural Changes in Human BMSCs after HK2 Cell-Extract Treatment

(A) Human BMSC morphology 24 hr after extract treatment (D1).

(B) Cobblestone morphology of the BMSCs 13 days (D13) after extract treatment.

(C) Epithelial colony 15 days (D15) after extract treatment.

(D) High magnification of the epithelial colony showing the cobblestone cell morphology.

(E and F) Dome formation (E, arrows) and tubular structures (F) after 25- and 35-day BMSC extract treatment (D25 and D35), respectively.

(G) Control HK2 cell morphology on the day of the extract preparation.

(H) Dome formation (arrows) under over-confluence culture conditions.

(I and J) BMSCs cultured in HK2 cell culture media at 24 hr (I, D1) and 35 days (J, D35).

Human BMSCs treated with HK2 cell extract form microvilli and tight intercellular contacts.

(K and L) Details of adjacent BMSCs treated with extracts grown on Thermanox for 35 days. Tight intercellular contacts are formed in BMSCs treated with HK2 cell extracts at D35 (arrowheads).

(M) Brush border formed in a BMSC treated with extract after 35 days.

(N–P) TEM images of HK2 cells (N and O) and BMSCs (P) grown in HK2 cell medium for 35 days (D35). Images are representative of two independent experiments.

Scale bars represent 200 μm (A), 50 μm (B and D–J), and 100 μm (C). Images are representative of three independent experiments.

Collectively, these studies revealed that following exposure with HK2 extracts, a subset of BMSCs acquire morphological, ultrastructural, and antigenic hallmarks of proximal tubular epithelial cells, suggesting that BMSC reprogramming was achieved using this treatment.

Reprogramming of BMSCs Requires Both Nuclear and Cytoplasmic Cell Extracts

In search of the component(s) of the cell extract responsible for reprogramming, we systematically analyzed nuclear and cytoplasmic extracts, extracts depleted of RNA, and proteins or treated with epigenetic modifiers such as trichostatin A and 5-aza-cytidine. Ablation of each of these components did not reproduce the effect of the whole-cell extract (Figure S2). These results are consistent with previously described data on the requirement of both nuclear and cytoplasmic cell extracts to achieve reprogramming (Håkelien et al., 2002).

Generation and Characterization of Clones from Reprogrammed BMSCs

To better characterize the human BMSCs treated with HK2 cell extracts, we next generated clones using a limiting-dilution approach. Of the 50 clones derived from one reprogrammed human BMSC experiment, the five that showed the most epithelial-like morphology were subjected to further analysis using qRT-PCR to examine their mesenchymal and epithelial marker profile. The expression

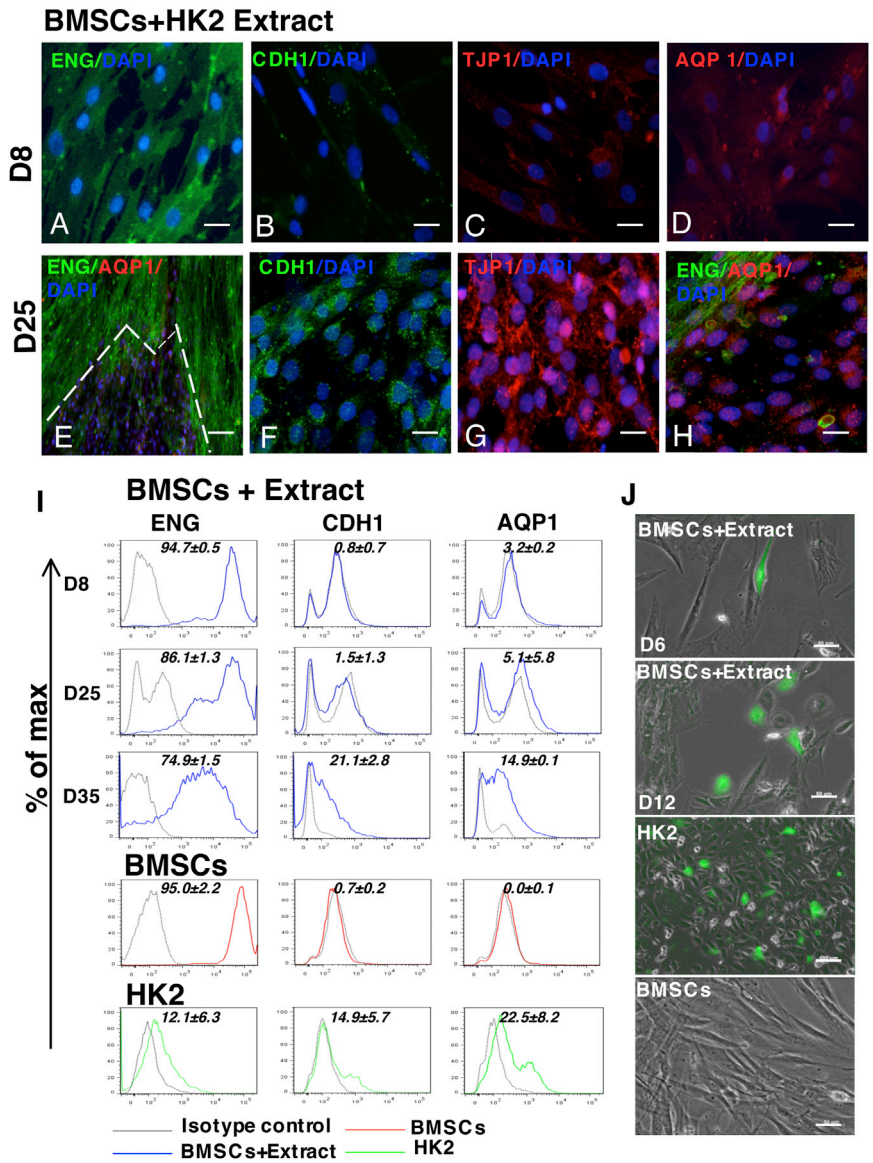

Figure 2. Antigenic Profile of Human BMSCs after HK2 Cell-Extract Treatment

(A–H) Expression of ENG, CDH1, TJP1, and AQP1 in BMSCs treated with extract at D8 (A–D) and D25 (E–H). (H) High-magnification view of the expression of ENG and AQP1 at the edge of the epithelial colony presented in (E). Scale bar, 50 μm. Representative images of three independent experiments.

(I) Representative FACS analysis of BMSCs treated with HK2 cell extract at different time points (D8, D25, and D35), and of untreated BMSCs and HK2 cells. Values are % of fluorescent cells (mean ± SD, n = 3 independent experiments).

(J) Representative images of CDH1/EGFP-positive cells 24 hr after transfection (days 6 and 12). Untreated BMSCs and HK2 cells are also shown. Scale bars represent 50 μm (BMSCs + extract [D6, D12] and BMSCs) and 100 μm (HK2). Transfection was performed in two independent reprogramming experiments (n = 2 for each time point).

See also Figure S1.

of *ENG*, *AQP1*, and gamma glutamyl transferase 1 (*GGT1*) in these five clones is depicted in Figure 3A. The difference in the expression of these markers reflects heterogeneity in reprogramming efficiency. Cells from clone 17 (CL17) were the most similar to HK2 cells and maintained a stable phenotype and morphology throughout passages. Expression of *AQP1* and *GGT1* mRNA has been also evaluated in primary proximal tubular epithelial cells (PTECs; Figure S3A). Consistent with the mRNA data, immunocytochemistry revealed that CL17 cells expressed TJP1, AQP1, and GGT1 proteins (Figure 3B). Scanning electron microscopy (SEM) revealed the presence of microvilli in CL17 similar to HK2 cells (Figure 3C). As expected, BMSCs did not show any microvilli (Figure 3C). Moreover, CL17 exhibited a duplication time comparable to that of HK2 cells (CL17: 20.4 ± 1.9 versus HK2: 18.9 ± 1.9 hr) and significantly shorter than BMSCs (55.2 ± 4.2 hr, Figure 3D). Altogether, these data indicated that the CL17, generated by BMSCs treated with the HK2 cell extracts, acquired the renal tubular epithelial phenotype.

Global Transcriptome Analysis in CL17, HK2, and BMSCs

To evaluate the global effect of BMSC reprogramming with cell extracts, we performed poly(A)+ mRNA deep sequencing in BMSCs and CL17 and HK2 cells (two biological replicates each). The homogeneity of the replicates of each cell type was confirmed by the high intra-group

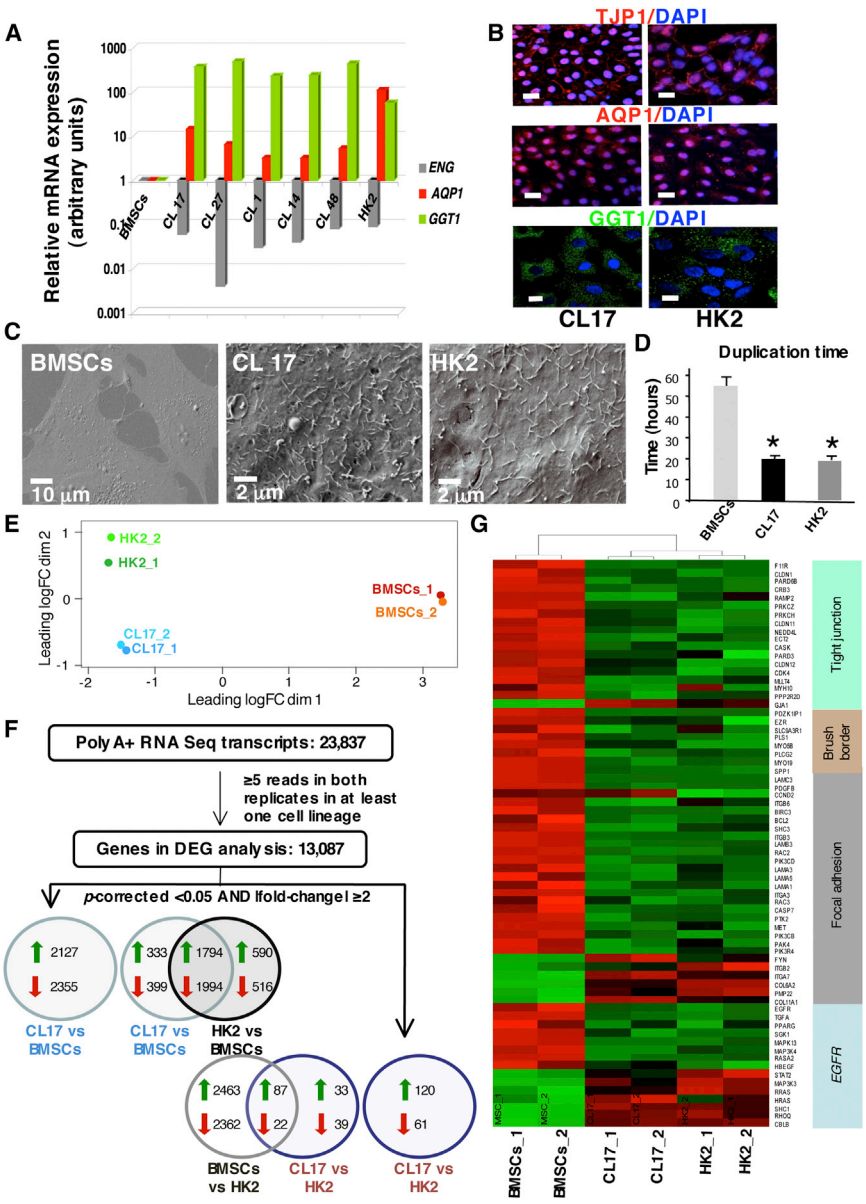

Figure 3. Characterization of Clones Generated by Human BMSCs after HK2 Cell-Extract Treatment

(A) Relative expression of *ENG*, *AQP1*, and *GGT1* mRNA by qRT-PCR in five selected clones and in HK2 cells compared to BMSCs. BMSC mRNA expression was used as the reference sample. Analyses were performed in triplicate. See also Figure S3A.

(B) Expression of TJP1, AQP1, and GGT1 proteins in clone 17 (CL17) and in HK2 cells. Scale bars, 50 µm.

(C) SEM analysis showed no microvilli in BMSCs. Instead, CL17 cells displayed microvilli similar to the HK2 cells. Representative images of three independent experiments.

(D) Duplication time (hours) in BMSCs, CL17 and HK2 cells (n = 5). Data are expressed as mean ± SD. *p < 0.01 versus BMSCs.

(E–G) RNA sequencing analysis of BMSCs and CL17 and HK2 cells. (E) Multidimensional scaling plot based on pairwise distances between global gene transcriptome profiles of six analyzed samples (two biological replicates for each cell lineages). (F) Workflow of transcriptome analysis showing the differentially expressed genes (DEGs) in BMSCs, CL17, and HK2 cells. At the intersection of the Venn diagrams, up- or downregulated genes both in CL17 and HK2 cells compared to BMSCs (top) and those up- or downregulated both in CL17 and BMSCs compared to HK2 cells (bottom) are reported. See also Table S3, which contains the full list of DEGs. The top 20 down- and upregulated genes and functionally characterized DEGs for selected pathways are reported in Tables S1, S2, and S3, respectively.

(G) Heatmap of the differentially expressed genes of the tight junction, brush border, focal adhesion, and *EGFR* networks. Columns represent biological replicates, and rows represent each gene. Green and red indicate high and low expression, respectively. The dendrogram of the unsupervised hierarchical clustering of the analyzed samples is shown in the upper part of the heatmap.

See also Figures S3–S5 and Tables S1, S2, and S3.

correlation coefficients (Figure S3B). Inter-group comparisons by scatterplots and Pearson coefficient correlations indicated a higher degree of similarity between reprogrammed CL17 cells and renal tubular HK2 cells (r = 0.957) than between the CL17 and BMSC cells (r = 0.605) (Figures S3C–S3E). Additionally, unsupervised hierarchical clustering of the six transcriptomes classified CL17 and HK2 cells together and separated them from BMSCs (Figure S4A). The same classification was obtained using multidimensional scaling, which is another unbiased method for measuring similarity between large datasets (Figure 3E). We further found more differentially expressed genes (DEGs) between CL17 and BMSCs (2,127 upregulated and 2,355 downregulated in CL17 compared to BMSCs) than between CL17 and HK2 cells (120 up- and 61 downregulated in CL17 relative to HK2). Remarkably, 85% of the CL17 up- or downregulated genes were consistently up- or downregulated in HK2 cells compared to BMSCs (Figure 3F).

Among the genes with the greatest fold change, there was a dramatic reduction in BMSC-related markers (i.e., *MMP2*, *TIMP3*, and *CDH11*) and increased expression of proximal tubular-cell-related markers (*F11R*, *SLCO4A1*, and *HNF1B*) (see full list in Tables S1 and S2). In addition, functional pathway analysis revealed in CL17 cells reduced levels of genes involved in mesenchymal cell-extracellular matrix interactions and increased levels of genes involved in proximal tubular cell-extracellular matrix interactions including laminins, collagens, and integrins (Table S3). Furthermore, CL17 showed upregulated expression of molecules involved in the tight junction and brush border as well as of several constituents involved in apical and basolateral structures of polarized proximal tubular cells (for the full list, see Table S3). The fold inductions observed using RNA sequencing were comparable to those obtained by qRT-PCR, with an R^2 correlation coefficient equal to 0.98, validating the approach (Figures S4B and S4C).

Functional network analysis of the upregulated genes involved in the process of proximal tubular cell polarization identified epidermal growth factor receptor (*EGFR*) as a candidate upstream regulator (Figures 3G and S5 and Table S3). Indeed, there was increased expression in CL17 of *EGFR* and its ligand, *TGFA*, as well as downstream targets such as *PRKCZ*, *PPARG*, and *SGK1*, which control tight junctions, some organic ion transporters, and regulators of apical membrane components (Panchapakesan et al., 2011). Remarkably, the above pathways were shared with HK2 cells (Figures 3G and S5 and Table S3).

Collectively, these data show that the reprogrammed CL17 cells lost mesenchymal markers and assumed an expression profile similar to renal tubular HK2 cells.

Functional Properties of CL17 Cells

Transepithelial Electrical Resistance

Having observed the formation of nascent intercellular contacts, we next inquired whether CL17 cells in addition to morphological and cell-lineage markers had acquired physiological properties similar to the epithelial phenotype. Testing the electrical resistance of BMSC monolayers showed trivial values of 34 ± 10 Ohm/cm^2. In contrast, monolayers of CL17 cells developed electrical resistance similar to that observed in HK2 cells (80 ± 10 versus 81 ± 12 Ohm/cm^2) (Figure 4A), both statistically significantly different from the transepithelial resistance (TER) assessed in BMSCs.

Albumin Binding and Uptake

Typical properties of proximal tubular epithelium are the binding and uptake of albumin in a receptor-dependent way (Gekle et al., 1998). Binding of BSA was studied in CL17, HK2, and BMSCs by exposing cells for 15 min to BSA and fluorescein isothiocyanate (FITC) alone or in the presence of an excess of cold BSA (Figure 4B, left panels) at 4°C, a condition known to prevent endocytotic processes and protein internalization (Ishibashi, 2004; Morigi et al., 2005; Takakura et al., 1995). As shown in Figure 4B (left panels), the addition of unlabeled albumin displaced BSA-FITC in CL17 to an extent comparable to HK2 cells, indicating the presence of specific binding sites for albumin in reprogrammed cells similar to the ones present in tubular epithelial cells (Figure 4B, left panels).

Uptake of albumin was assessed in cells exposed to BSA-FITC alone or in the presence of an excess of unlabeled BSA at 37°C for 90 min, an experimental condition previously described as allowing appreciable protein endocytosis (Ishibashi, 2004; Morigi et al., 2005; Takakura et al., 1995) (Figure 4B, right panels). Albumin uptake was markedly inhibited by an excess of unlabeled protein, suggesting receptor-mediated endocytosis of BSA-FITC in CL17 comparable to that observed in HK2 cells (Figure 4B, right panel). Control BMSCs did not exhibit any binding or uptake of BSA-FITC (Figure 4B, bottom panels).

Altogether, these studies revealed that CL17 cells acquired and maintained functional properties of proximal tubular-like epithelial cells.

CL17 Cells Contribute to Tubular Structures in Renal Organoids Ex Vivo

To assess the functional integration into kidney tissue, human cells (CL17, HK2, or BMSCs) were mixed with kidney cells derived from embryonic day 11.5 (E11.5) mice (Unbekandt and Davies, 2010; Xinaris et al., 2012), and grown as explants for 5 days. At day 1, CL17 cells integrated into the condensing metanephric mesenchyme that was identified by co-expression of neural cell adhesion molecule (NCAM) and PAX2 markers (Figure 5A, insert). At day 5, chimeric aggregates of human and mouse cells grew into elongating tubular structures that were surrounded by laminin-positive basement membranes (Figures 5B and 5C). Remarkably, tubular structures containing CL17 or HK2 cells were in close vicinity to glomerular-like structures expressing the early podocyte marker Wilms tumor 1 (WT1) (Figures 5E and 5F). BMSCs neither formed nor contributed to renal structures, indicating non-nephrogenic potential (Figures 5D and 5G).

CL17 Cells Engraft into Proximal Tubuli and Reduce Renal Damage in AKI Mice

The renoprotective potential of the reprogrammed cells was investigated in an experimental murine model of cisplatin-induced AKI (Morigi et al., 2008). After intravenous injection of CL17 cells, 50% were recovered in the lung, 1% in the spleen, 0.47% in the liver, and 21% in the kidney; no cells were found in the heart (Figure S6A). Engrafted CL17 cells, stained for two human markers for mitochondria and centromere protein-A (CENP-A), in the renal parenchyma of immunodeficient

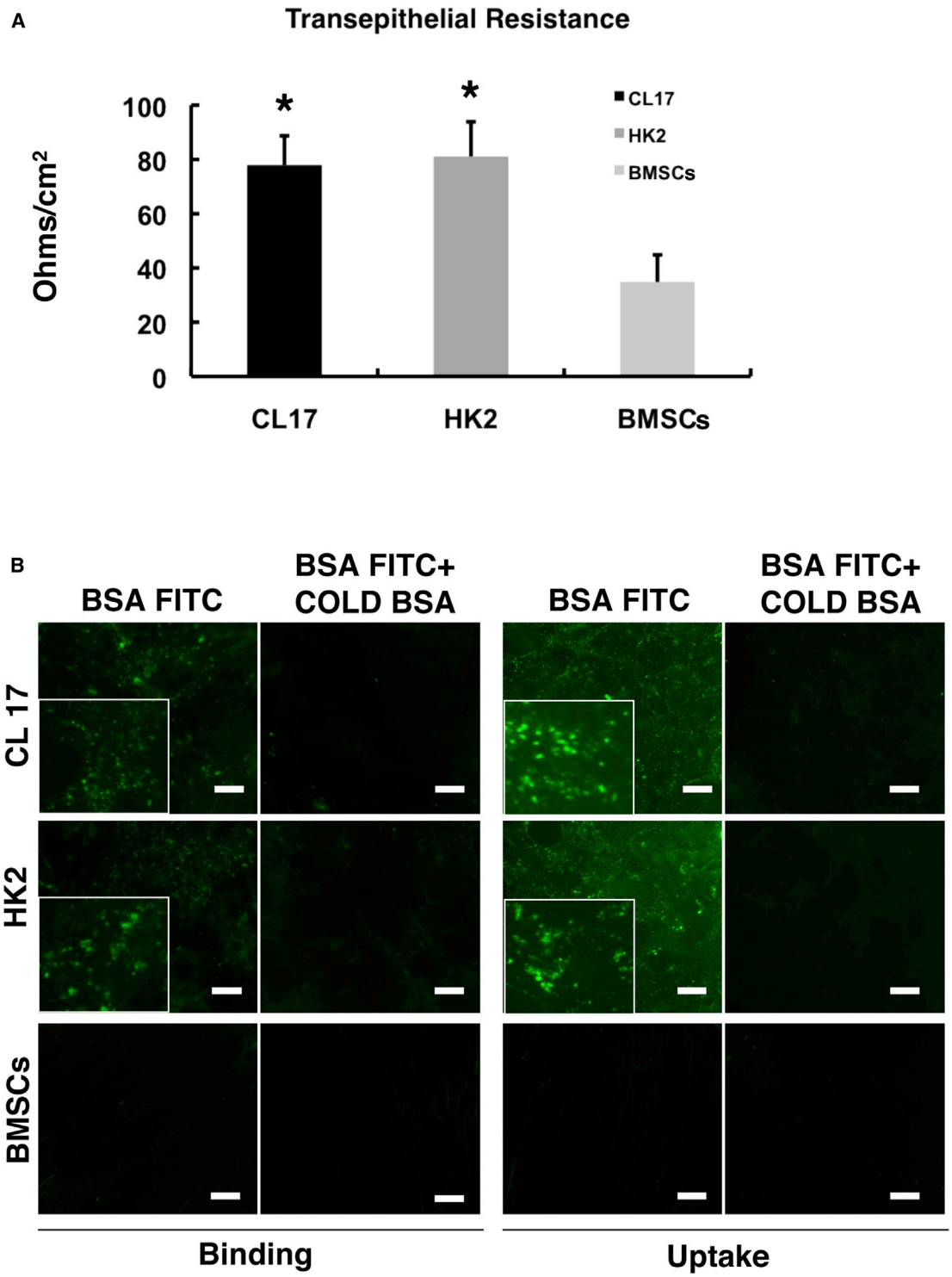

Figure 4. Functional Properties of CL17 Cells In Vitro

(A) Transepithelial resistance (TER) measurement of CL17, HK2, and BMSCs. Three independent experiments were done in duplicate. Data are expressed as mean ± SD; *$p < 0.01$ versus BMSCs.

(B) BSA binding and uptake in CL17, HK2, and BMSCs. Cells were exposed to 50 μg/ml BSA-FITC alone or in the presence of excess cold BSA (5 mg/ml) for 15 min at 4°C for binding experiments (left) and for 90 min at 37°C for uptake experiments (right). Images are representative of three experiments. Scale bars, 50 μm.

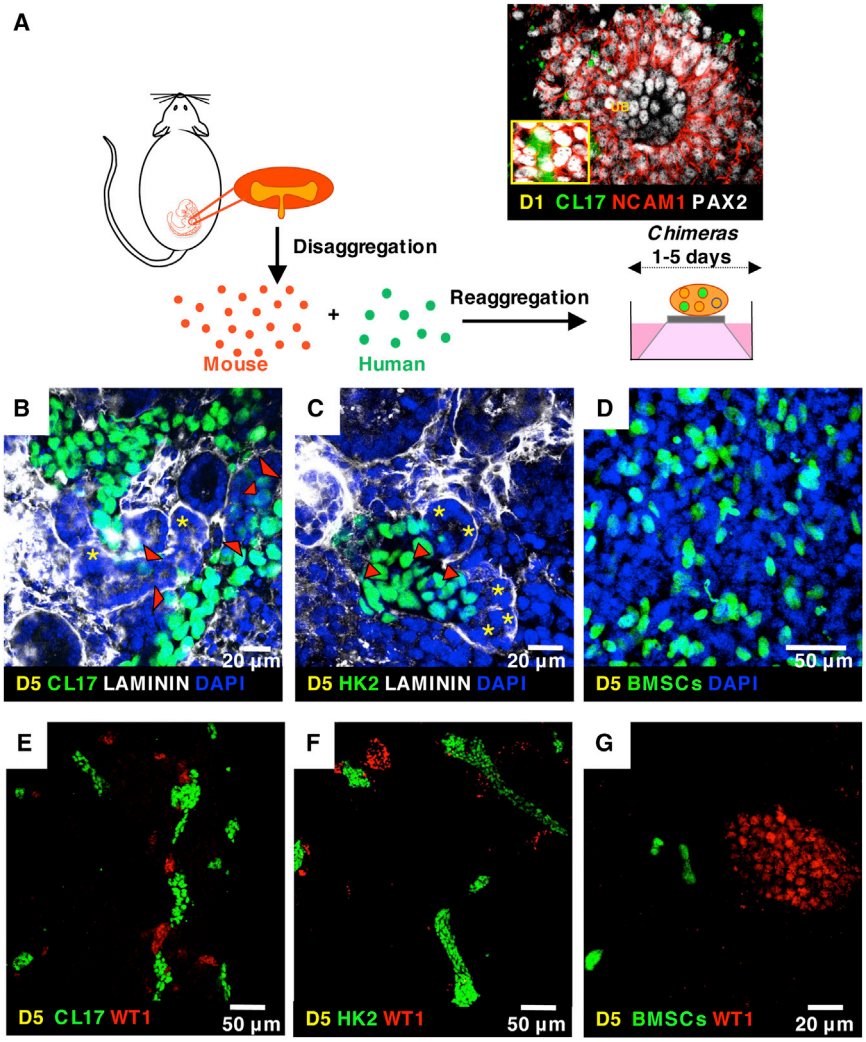

Figure 5. Human CL17, HK2, and BMSC Integration in Renal Organoids

(A) Human CL17, HK2, or BMSCs were mixed with fully dissociated E11.5 mouse embryonic kidneys and grown as explants for 1–5 days. Representative image of CL17-cell integration (stained with Cell Tracker, green) into the condensing metanephric mesenchyme identified by NCAM1 and PAX2 co-staining at day 1 (insert image).

(B and C) At day 5, chimeric aggregates of human (immunostained with anti human nuclear antigen, green; arrowhead) and mouse cells (asterisk) lay within laminin-positive membranes (white). Cell nuclei were labeled with DAPI (blue).

(E and F) CL17 cells (E) and HK2 cells (F) form elongating tubular structures in the vicinity of WT1-positive glomerular structures.

(D and G) BMSCs never formed any renal structure. Images are representative of three independent experiments.

AKI mice, were localized in the tubular compartment at 4 days post-cisplatin injection (Figure 6A) with a frequency averaging 213 PKH26^{+ve} cells/100,000 renal cells. CL17 cells predominantly localized within proximal tubuli (80%) and, to a lesser extent (20%), in the peritubular areas (Figure 6B). As a positive control for human markers, we used human BMSCs that were mainly found at the peritubular level in tissues of cisplatin-treated mice (Figure S6B). Negative controls with non-immune immunoglobulin of the same isotype as the primary antibody are shown in Figure S6C. Next, we studied the effect of CL17 cell treatment on renal function impairment and tubular damage. In cisplatin-treated mice given CL17 cells, renal function was ameliorated (Figure 6C), although blood urea nitrogen (BUN) levels were not significantly different from those observed in untreated animals (22 ± 2 mg/dl) at 4 days. In parallel, renal damage was significantly improved in AKI animals infused with CL17 cells as demonstrated by the significant reduction of hyaline casts and necrotic tubuli (Figures 6D and 6E). Control mice did not show any signs of tubular damage. Altogether, these data indicate that the reprogrammed BMSCs directly incorporated into proximal tubuli and improved renal damage and function in AKI mice.

DISCUSSION

Our results provide evidence that human BMSCs can be directly reprogrammed into cells that closely resemble renal proximal tubular epithelial cells using cell extracts. The reprogramming of BMSCs is demonstrated by the acquisition of (1) morphological, ultrastructural, and antigenic properties; (2) transcriptomic profile; and (3) functional characteristics of proximal tubular-like epithelial cells. Notably, the directly reprogrammed cells acquire

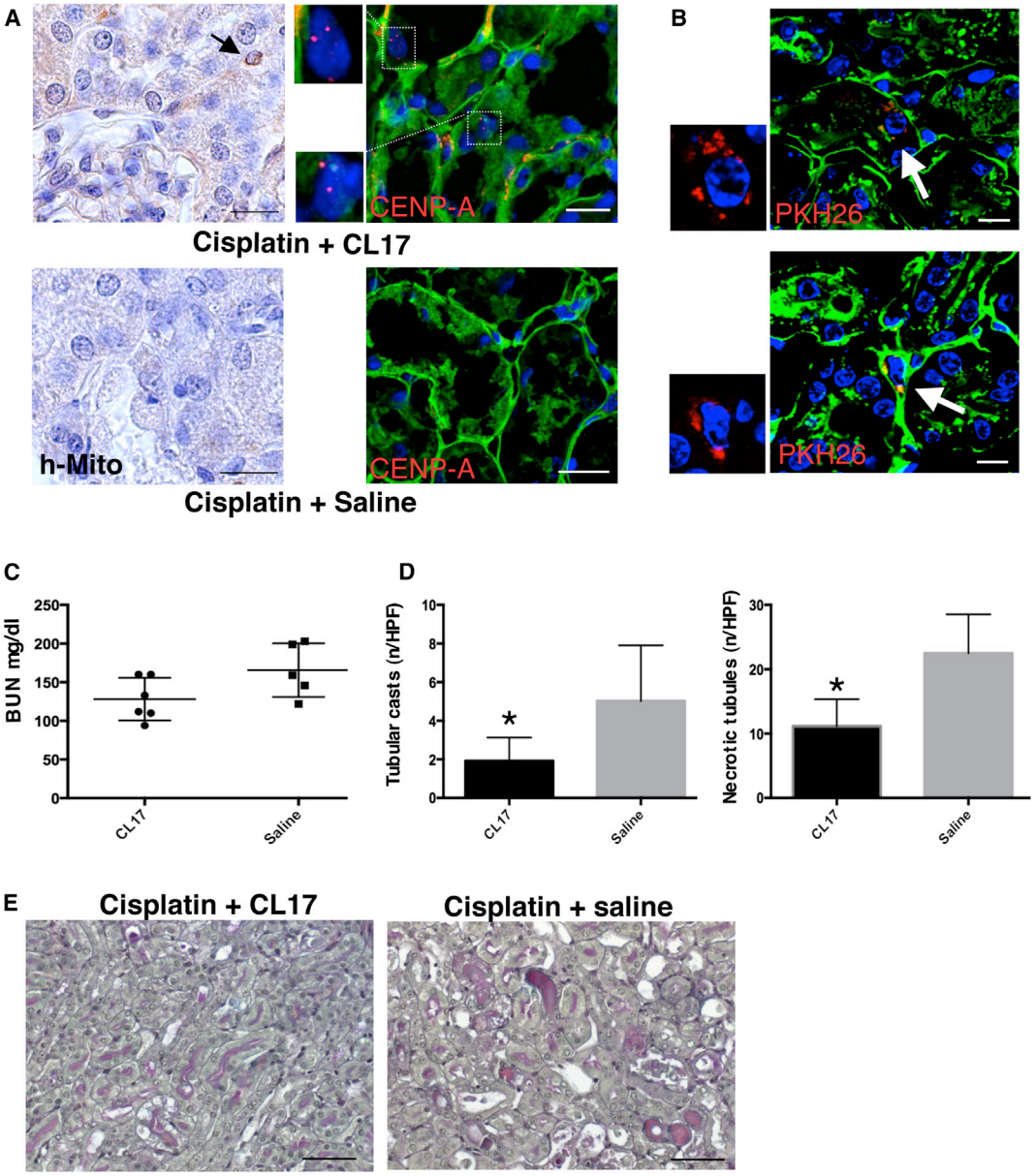

Figure 6. CL17 Cells Engrafted in Proximal Tubuli in Mice with Cisplatin-Induced AKI

(A) Incorporation of CL17 cells into kidney tubuli of mice with cisplatin-induced AKI detected by human mitochondrial (h-Mito, upper-left panel; brown) and CENP-A (upper-right panel and insets; red) staining. Arrow indicates an h-Mito-positive cell in the proximal tubule connected to the glomerulus. No h-Mito- and CENP-A-positive cells are present in renal tissue of AKI animals with saline (bottom). DAPI (blue) stains nuclei, and renal structures are labeled with wheat germ agglutinin (WGA, green). Scale bars represent 10 μm for h-Mito staining and 20 μm for CENP-A staining.

(B) Renal localization of PKH26/positive CL17 cells (red) in AKI mice within proximal tubuli (top) or in peritubular areas (bottom). DAPI (blue) stains nuclei, and renal structures are labeled with WGA (green). Scale bars, 20 μm.

(C) Blood urea nitrogen (BUN) (mg/dl) levels in AKI mice treated with CL17 cells (n = 6) or saline (n = 5) at 4 days. Data are expressed as mean ± SD.

(D) Quantification of tubular casts and necrotic tubuli (n/high-power field [HPF]) in kidneys of AKI mice treated with CL17 cells or saline at 4 days. *$p < 0.05$ versus cisplatin + saline.

(E) Representative histological micrographs of the kidney of the AKI animals treated with CL17 cells (left) or saline (right) at 4 days. Scale bar, 50 μm.

See also Figure S6.

epithelial features and gain organ-forming capacity and have functional properties to the extent that they reduced renal damage in experimental AKI.

Several strategies have been adopted to achieve reprogramming, namely, iPSC technology, SCNT, cell fusion, and cell-extract treatment (Gurdon, 2006; Håkelien et al., 2002; Tada et al., 1997; Takahashi and Yamanaka, 2006). Among these approaches, the use of cell extracts has gained attention because it is an oocyte-independent reprogramming method devoid of ethical and legal concerns and does not pass through the pluripotent state, which is an emerging desirable scientific goal.

Here, we used human BMSCs, an attractive cell population for clinical application due to their accessibility, expansion potential, genetic stability, and the presence of an unmethylated genome, which render them prone to reprogramming (Bianco et al., 2013; Le Blanc and Mougiakakos, 2012; Morigi and Benigni, 2013; Morigi et al., 2008; Streckfuss-Bömeke et al., 2013). Our work provides evidence that human BMSCs can be reprogrammed into a developmentally distinct tubular lineage based on multifaceted approaches spanning from cell morphology documented using transmission and scanning electron microscopy to mRNA sequencing revealing an abundance of tubular epithelial transcripts and expression of proteins characteristic of renal proximal tubular cells. The paradigm that BMSCs can be driven toward a renal fate, also evidenced by the acquisition of proximal tubular functional competence such as TER and albumin binding and uptake activity, points the way to an efficient methodology for generating renal cell types by using a readily available autologous cell source.

In search of mechanisms responsible for BMSC reprogramming, we attempted to uncover the actual blueprint for reprogramming, which resides in the cell-free extract of tubular epithelia, by depleting it of various putative mediators of the process. Specifically, the requirement for the combination of nuclear and cytoplasmic factors is disclosed. Moreover, reprogramming does not occur if deproteinated or RNA-depleted extracts are used.

The use of a kidney re-aggregation assay (Xinaris et al., 2012), which represents a stringent ex vivo model for the evaluation of the renal potential of a test population (Hendry et al., 2013), contributes to further proving the identity of the reprogrammed BMSCs. Reprogrammed cells in the presence of embryonic kidney cells showed a remarkable ability to form three-dimensional chimeric tubular structures, indicating the efficient switch toward a renal cell phenotype. Importantly, the reprogramming of BMSCs toward a renal lineage reported herein may have clinical applications in the future. Cell treatment with reprogrammed BMSCs partly improved renal function and significantly limited tubular injury in mice with AKI. This beneficial effect is ascribed to the high engraftment and integration of infused cells into damaged proximal tubuli of AKI mice. Such integration does not occur when animals with AKI are infused with BMSCs, which preferentially localize at the peritubular space (Humphreys and Bonventre, 2008; Morigi and Benigni, 2013; Morigi et al., 2008), highlighting the different nature of reprogrammed versus native BMSCs. Another peculiar feature of reprogrammed BMSCs was their localization in different organs after systemic infusion. In nonobese diabetic severe combined immunodeficiency mice with AKI, reprogrammed BMSCs were detected and/or entrapped predominantly in lung and, to a very low extent, in the spleen and the liver, while native BMSCs were found in limited numbers in these organs (François et al., 2006; Tögel et al., 2005). A corollary of the present results are previous reports demonstrating improved survival and augmented kidney function in rodent models of kidney disease after injection with a mixed renal tubular cell population (Kelley et al., 2010).

Extract-induced reprogramming, by virtue of the high yield, permits the derivation of a large number of isogenic renal cell clones. Moreover, these cells can be stored and retrieved upon request without losing their identity. Thus, the reprogrammed BMSCs can be a tool for drug screening and toxicological assays.

In summary, reprogramming BMSCs with the cell-free extracts of epithelial or other fully differentiated somatic cells, when successful, brings to the fore the flexibility and choice of designer engineering. This approach and its future refinements could potentially fulfill the quest to utilize somatic cell types in a precursor state for durable cell therapy.

EXPERIMENTAL PROCEDURES

Cell Culture

The human immortalized proximal tubular cell line HK2 (CRL-2190, ATCC) was cultured in keratinocyte serum-free medium (Clonetics, Life Technologies) supplemented with bovine pituitary extract and epidermal growth factor. Experiments were performed at passages 20–40. Human BMSCs from two different donors were obtained from the Transplantation Program of the Haematology Division of Azienda Ospedaliera Papa Giovanni XXIII, Bergamo, Italy. Cells were cultured as previously described (Capelli et al., 2007) using low-glucose DMEM (Sigma-Aldrich) supplemented with 5% human platelet lysate. Experiments were performed at passages 4–6.

Cell Extracts

HK2 cell extracts were prepared as previously described (Håkelien et al., 2002). In brief, ~100 × 10^6 cells were washed twice in ice-cold PBS and once in cold cell lysis buffer (10 mM HEPES [pH 8.2], 50 mM NaCl, 5 mM $MgCl_2$, 1 mM DTT, and 1:100 protease inhibitors; all from Sigma-Aldrich) sedimented at 300 × *g* for 10 min at 4°C. The volume of cell pellet was added with an equal

volume of cold lysis buffer and incubated for 45 min on ice. Cells were sonicated on ice in 200-μl aliquots using a sonicator fitted with a 2-mm diameter probe (60% output; Heat Systems) until all cells and nuclei were lysed, as judged by microscopy. The lysate was sedimented at 15,000 × *g* for 15 min at 4°C. The supernatant was aliquoted in 100-μl aliquots and used immediately for reprogramming assays of 100,000 BMSCs.

SLO Permeabilization and Cell-Extract Treatment

Preliminary experiments were performed in order to define the optimal concentration of SLO (Sigma-Aldrich) for BMSCs using concentrations of 100, 200, 300, 400, 500, 600, 700, and 800 ng/ml. Permeabilization efficiency of >80% was obtained at 400 ng/ml, as assessed by monitoring the uptake of an *M*r 70,000 Texas-red-conjugated dextran (50 μg/ml; Molecular Probes, Invitrogen). Cell viability, assessed by trypan blue exclusion assay, was not affected by the chosen SLO concentration. BMSCs were washed twice in cold PBS and once in ice cold Ca^{2+}- and Mg^{2+}-free Hank's balanced salt solution (HBSS; Gibco, Invitrogen). Cells were resuspended in aliquots of 100,000 cells in HBSS in 1.5-ml tubes and centrifuged at 1,500 rpm for 5 min at 4°C. Cells were suspended in ice-cold HBSS containing 400 ng/ml SLO and incubated for 50 min at 37°C and finally centrifuged at 1,500 rpm for 5 min at 4°C. Permeabilized BMSCs were exposed to HK2 cell extract containing an ATP-regenerating system (1 mmol/l ATP, 10 mmol/l creatine phosphate, 25 μg/ml creatine kinase; 100 μmol/l GTP; all from Sigma-Aldrich) and 1 mmol/l of each nucleotide triphosphate (Roche Diagnostics) and incubated for 1 hr at 37°C. So that BMSC membranes could be resealed, the cell suspension was diluted with HK2 cell medium containing 2 mM $CaCl_2$, and cells were seeded in a six-well plate. As a control, permeabilized BMSCs were grown in HK2 cell medium. Where needed, HK2 cell extracts were incubated as follows: (1) at 100°C for 5 min or (2) with 100 μg/ml RNase A (Roche diagnostics) for 30 min, followed by 1 hr incubation with RNase inhibitor (1 μg/μl; Ambion, Invitrogen). In some experiments, HK2 cells were treated with 25 nM trichostatin A or 50 nM 5-aza-cytidine (both from Sigma-Aldrich) or both 48 hr before preparing the extract (Rajasingh et al., 2011). The reprogramming experiments were repeated successfully 15 out of 17 times with human BMSCs from two different donors, generating epithelial cells at the same timing as observed with light microscopy (i.e., 13–15 days).

CDH1 EGFP Transfection

CDH1 EGFP plasmid was obtained commercially (Genecopeia; HPRM12692-PF02). Human BMSCs, BMSCs treated with HK2 cell extracts (at days 5 and 11 post reprogramming assay), and HK2 cells grown on six-well plates were transfected with 2.5 μg of plasmid using lipofectamine 2000 (Invitrogen, Life Technologies) according to the manufacturer's instructions. Representative images were taken 24 hr post-transfection (days 6 and 12) using an Apotome microscope (Axion Vision, Imager 2Z, Zeiss).

RNA Sequencing

Two biological replicates were performed for each cell lineage. Poly(A)+ RNA was obtained from 20 μg of total RNA using the Dynabeads mRNA DIRECT Micro Kit after adding external RNA spike-in controls (External RNA Controls Consortium). Libraries were prepared using the Ion Total RNA-Seq Kit v2. Template preparation and sequencing were performed using the Ion PGM Template OT2 200 Kit and the Ion PGM Sequencing 200 Kit v2. Each replicate was sequenced on the Ion PGM Sequencer using an Ion 318 Chip. Data extraction, base calling, and alignment were performed using TorrentSuite Software 3.6. To count reads overlapping with known exon coordinates (RefSeq, UCSC Genome Browser), we used the HTSeq software through a modified version of the FeatureCounter plugin that allowed it to discard reads with mapping quality score < 5. Differential expression analyses were performed on genes showing five or more reads in both replicates in at least one cell lineage using edgeR and RobiNA software. Functional pathway analysis was performed with the GraphiteWeb and the ToppFun softwares using a two-step strategy. First, we analyzed genes showing the most striking changes, defined as $p \leq 0.05$ (with Benjamini-Hochberg multiple testing correction), $\geq$10-fold change, and expression levels of three or more reads per kilobase per million in at least one cell lineage. Second, we analyzed all genes with p-corrected ≤ 0.05 and $\geq$ 2-fold change.

TER Measurement

Human BMSCs and CL17 and HK2 cells were plated in 24-well transwell filters of 0.2 μm pore size (Corning) at a concentration of 250,000/0.5 ml in triplicate. Cells were used for TER measurement (Millicell ERS; Millipore) 48 hours after reaching confluency. TER (Ohm/cm^2) was measured at 37°C, and measurements were performed twice every 10 min according to the manufacturer's instructions.

In Vivo Experiments

Female 2-month-old NOD.CB17-Prkdc scid/NcrCrl (NOD-SCID) mice (Charles River Italia) were used. Animal care and treatment were conducted in conformity with institutional guidelines and international laws and policies (Morigi et al., 2011). Animal studies were approved by the institutional animal care and use committees of Mario Negri Institute, Milan, Italy.

AKI was set up in NOD-SCID mice by subcutaneous injection of the nephrotoxic drug cisplatin (Ebewe Italia) at a dose of 13 mg/kg as previously described (Morigi et al., 2008). For investigation of the effect of reprogrammed cells (CL17), 24 hr after cisplatin injection, mice received intravenous (tail vein) saline (n = 5) or CL17 cells at passage 16 (n = 6). Mice were injected with 5 × 10^5 cells (50% of cells were labeled with PKH26, Sigma-Aldrich). This experiment was performed once. The animals were euthanized 4 days after cisplatin injection, and kidney, lung, heart, spleen, and liver were used for histology and immunohistochemistry evaluation. Cell engraftment was evaluated in paraformaldehyde-lysine-periodate-fixed cryosections.

Renal function was assessed using blood urea nitrogen (BUN) levels measured by the Reflotron test (Roche Diagnostics). Basal BUN levels of NOD-SCID mice averaged 22 ± 2 mg/dl. BUN levels exceeding this range of values were considered abnormal.

Statistical Analysis

Results are expressed as mean ± SD. Data were analyzed using the t test for unpaired data. Statistical significance was defined as $p < 0.05$.

See the Supplemental Experimental Procedures for details regarding the generation of clones using limiting dilution and duplication time measurement, transmission electron microscopy and scanning electron microscopy, immunocytochemistry and flow cytometry, renal histology and immunohistochemistry analysis, RNA extraction and qRT-PCR, albumin binding and uptake assays, and renal organoids.

ACCESSION NUMBERS

The GEO repository accession number for the RNA-sequencing data reported in this paper is GSE56625.

SUPPLEMENTAL INFORMATION

Supplemental Information includes Supplemental Experimental Procedures, six figures, and three tables and can be found with this article online at http://dx.doi.org/10.1016/j.stemcr.2015.02.002.

AUTHOR CONTRIBUTIONS

E.P. conceived and designed the study, collected and/or assembled data, performed data analysis and interpretation, wrote the manuscript, and gave final approval of the manuscript. M.M, G.R., and M.S.G. conceived and designed the study, analyzed and interpreted data, wrote the manuscript, and gave final approval of the manuscript. P.I., C.X., V.B., S.T., L.L., C.R., M.T., P.R., and M.G.S. collected and/or assembled data, performed data analysis and interpretation, wrote the manuscript, and gave final approval of the manuscript. M.I. provided study materials. A.B. conceived and designed the study, performed data analysis and interpretation, wrote the manuscript, gave final approval of the manuscript, and provided financial support.

ACKNOWLEDGMENTS

We would like to thank Drs. Chiara Capelli, Daniela Cavallotti, Debora Conti, Daniela Corna, Miriam Galbusera, Rubina Novelli, Serge Cedrick Mbiandjeu Toya, Piera Trionfini, Franca Orsini, Luca Perico, and Anna Pezzotta for their great contributions and excellent technical assistance. Manuela Passera assisted in the preparation of the manuscript. This work was supported by Fondazione Cariplo (grant 2011-1642) and partially supported by a European Commission grant (project STELLAR n. HEALTH-FP-2012-305436). M.S.G. was partially supported by the NIH (grants DK54602, DK052783, and DK45462) and the Westchester Artificial Kidney Foundation. Valentina Benedetti and Paola Rizzo are recipients of fellowships from Fondazione Aiuti per la Ricerca sulle Malattie Rare (ARMR), Bergamo, Italy. The monoclonal antibody anti-NCAM, 5B8, developed by Thomas M. Jessell and Jane Dodd, was obtained from the Developmental Studies Hybridoma Bank developed under the auspices of the NICHD and maintained by the University of Iowa, Department of Biological Sciences, Iowa City, IA 52242.

Received: May 2, 2014
Revised: February 3, 2015
Accepted: February 4, 2015
Published: March 5, 2015

REFERENCES

Angelotti, M.L., Ronconi, E., Ballerini, L., Peired, A., Mazzinghi, B., Sagrinati, C., Parente, E., Gacci, M., Carini, M., Rotondi, M., et al. (2012). Characterization of renal progenitors committed toward tubular lineage and their regenerative potential in renal tubular injury. Stem Cells *30*, 1714–1725.

Benigni, A., Morigi, M., and Remuzzi, G. (2010). Kidney regeneration. Lancet *375*, 1310–1317.

Bianco, P., Cao, X., Frenette, P.S., Mao, J.J., Robey, P.G., Simmons, P.J., and Wang, C.Y. (2013). The meaning, the sense and the significance: translating the science of mesenchymal stem cells into medicine. Nat. Med. *19*, 35–42.

Capelli, C., Domenghini, M., Borleri, G., Bellavita, P., Poma, R., Carobbio, A., Micò, C., Rambaldi, A., Golay, J., and Introna, M. (2007). Human platelet lysate allows expansion and clinical grade production of mesenchymal stromal cells from small samples of bone marrow aspirates or marrow filter washouts. Bone Marrow Transplant. *40*, 785–791.

François, S., Bensidhoum, M., Mouiseddine, M., Mazurier, C., Allenet, B., Semont, A., Frick, J., Saché, A., Bouchet, S., Thierry, D., et al. (2006). Local irradiation not only induces homing of human mesenchymal stem cells at exposed sites but promotes their widespread engraftment to multiple organs: a study of their quantitative distribution after irradiation damage. Stem Cells *24*, 1020–1029.

Gaustad, K.G., Boquest, A.C., Anderson, B.E., Gerdes, A.M., and Collas, P. (2004). Differentiation of human adipose tissue stem cells using extracts of rat cardiomyocytes. Biochem. Biophys. Res. Commun. *314*, 420–427.

Gekle, M., Mildenberger, S., Freudinger, R., and Silbernagl, S. (1998). Long-term protein exposure reduces albumin binding and uptake in proximal tubule-derived opossum kidney cells. J. Am. Soc. Nephrol. *9*, 960–968.

Ginsberg, M., James, D., Ding, B.S., Nolan, D., Geng, F., Butler, J.M., Schachterle, W., Pulijaal, V.R., Mathew, S., Chasen, S.T., et al. (2012). Efficient direct reprogramming of mature amniotic cells into endothelial cells by ETS factors and TGFβ suppression. Cell *151*, 559–575.

Gurdon, J.B. (2006). From nuclear transfer to nuclear reprogramming: the reversal of cell differentiation. Annu. Rev. Cell Dev. Biol. *22*, 1–22.

Håkelien, A.M., Landsverk, H.B., Robl, J.M., Skålhegg, B.S., and Collas, P. (2002). Reprogramming fibroblasts to express T-cell functions using cell extracts. Nat. Biotechnol. *20*, 460–466.

Håkelien, A.M., Gaustad, K.G., and Collas, P. (2004). Transient alteration of cell fate using a nuclear and cytoplasmic extract of an insulinoma cell line. Biochem. Biophys. Res. Commun. *316*, 834–841.

Hendry, C.E., Vanslambrouck, J.M., Ineson, J., Suhaimi, N., Takasato, M., Rae, F., and Little, M.H. (2013). Direct transcriptional reprogramming of adult cells to embryonic nephron progenitors. J. Am. Soc. Nephrol. *24*, 1424–1434.

Humphreys, B.D., and Bonventre, J.V. (2008). Mesenchymal stem cells in acute kidney injury. Annu. Rev. Med. *59*, 311–325.

Ieda, M., Fu, J.D., Delgado-Olguin, P., Vedantham, V., Hayashi, Y., Bruneau, B.G., and Srivastava, D. (2010). Direct reprogramming of fibroblasts into functional cardiomyocytes by defined factors. Cell *142*, 375–386.

Ishibashi, F. (2004). High glucose reduces albumin uptake in cultured proximal tubular cells (LLC-PK1). Diabetes Res. Clin. Pract. *65*, 217–225.

Karow, M., Sánchez, R., Schichor, C., Masserdotti, G., Ortega, F., Heinrich, C., Gascón, S., Khan, M.A., Lie, D.C., Dellavalle, A., et al. (2012). Reprogramming of pericyte-derived cells of the adult human brain into induced neuronal cells. Cell Stem Cell *11*, 471–476.

Kelley, R., Werdin, E.S., Bruce, A.T., Choudhury, S., Wallace, S.M., Ilagan, R.M., Cox, B.R., Tatsumi-Ficht, P., Rivera, E.A., Spencer, T., et al. (2010). Tubular cell-enriched subpopulation of primary renal cells improves survival and augments kidney function in rodent model of chronic kidney disease. Am. J. Physiol. Renal Physiol. *299*, F1026–F1039.

Lam, A.Q., Freedman, B.S., Morizane, R., Lerou, P.H., Valerius, M.T., and Bonventre, J.V. (2014). Rapid and efficient differentiation of human pluripotent stem cells into intermediate mesoderm that forms tubules expressing kidney proximal tubular markers. J. Am. Soc. Nephrol. *25*, 1211–1225.

Landsverk, H.B., Håkelien, A.M., Küntziger, T., Robl, J.M., Skålhegg, B.S., and Collas, P. (2002). Reprogrammed gene expression in a somatic cell-free extract. EMBO Rep. *3*, 384–389.

Le Blanc, K., and Mougiakakos, D. (2012). Multipotent mesenchymal stromal cells and the innate immune system. Nat. Rev. Immunol. *12*, 383–396.

Lin, S.A., Kolle, G., Grimmond, S.M., Zhou, Q., Doust, E., Little, M.H., Aronow, B., Ricardo, S.D., Pera, M.F., Bertram, J.F., and Laslett, A.L. (2010). Subfractionation of differentiating human embryonic stem cell populations allows the isolation of a mesodermal population enriched for intermediate mesoderm and putative renal progenitors. Stem Cells Dev. *19*, 1637–1648.

Mae, S., Shono, A., Shiota, F., Yasuno, T., Kajiwara, M., Gotoda-Nishimura, N., Arai, S., Sato-Otubo, A., Toyoda, T., Takahashi, K., et al. (2013). Monitoring and robust induction of nephrogenic intermediate mesoderm from human pluripotent stem cells. Nat. Commun. *4*, 1367.

McGann, C.J., Odelberg, S.J., and Keating, M.T. (2001). Mammalian myotube dedifferentiation induced by newt regeneration extract. Proc. Natl. Acad. Sci. USA *98*, 13699–13704.

Morigi, M., and Benigni, A. (2013). Mesenchymal stem cells and kidney repair. Nephrol. Dial. Transplant. *28*, 788–793.

Morigi, M., Buelli, S., Angioletti, S., Zanchi, C., Longaretti, L., Zoja, C., Galbusera, M., Gastoldi, S., Mundel, P., Remuzzi, G., and Benigni, A. (2005). In response to protein load podocytes reorganize cytoskeleton and modulate endothelin-1 gene: implication for permselective dysfunction of chronic nephropathies. Am. J. Pathol. *166*, 1309–1320.

Morigi, M., Introna, M., Imberti, B., Corna, D., Abbate, M., Rota, C., Rottoli, D., Benigni, A., Perico, N., Zoja, C., et al. (2008). Human bone marrow mesenchymal stem cells accelerate recovery of acute renal injury and prolong survival in mice. Stem Cells *26*, 2075–2082.

Morigi, M., Galbusera, M., Gastoldi, S., Locatelli, M., Buelli, S., Pezzotta, A., Pagani, C., Noris, M., Gobbi, M., Stravalaci, M., et al. (2011). Alternative pathway activation of complement by Shiga toxin promotes exuberant C3a formation that triggers microvascular thrombosis. J. Immunol. *187*, 172–180.

Panchapakesan, U., Pollock, C., and Saad, S. (2011). Renal epidermal growth factor receptor: its role in sodium and water homeostasis in diabetic nephropathy. Clin. Exp. Pharmacol. Physiol. *38*, 84–88.

Qian, L., Huang, Y., Spencer, C.I., Foley, A., Vedantham, V., Liu, L., Conway, S.J., Fu, J.D., and Srivastava, D. (2012). In vivo reprogramming of murine cardiac fibroblasts into induced cardiomyocytes. Nature *485*, 593–598.

Qin, M., Tai, G., Collas, P., Polak, J.M., and Bishop, A.E. (2005). Cell extract-derived differentiation of embryonic stem cells. Stem Cells *23*, 712–718.

Qu, T., Shi, G., Ma, K., Yang, H.N., Duan, W.M., and Pappas, G.D. (2013). Targeted cell reprogramming produces analgesic chromaffin-like cells from human mesenchymal stem cells. Cell Transplant. *22*, 2257–2266.

Rajasingh, J., Lambers, E., Hamada, H., Bord, E., Thorne, T., Goukassian, I., Krishnamurthy, P., Rosen, K.M., Ahluwalia, D., Zhu, Y., et al. (2008). Cell-free embryonic stem cell extract-mediated derivation of multipotent stem cells from NIH3T3 fibroblasts for functional and anatomical ischemic tissue repair. Circ. Res. *102*, e107–e117.

Rajasingh, J., Thangavel, J., Siddiqui, M.R., Gomes, I., Gao, X.P., Kishore, R., and Malik, A.B. (2011). Improvement of cardiac function in mouse myocardial infarction after transplantation of epigenetically-modified bone marrow progenitor cells. PLoS ONE *6*, e22550.

Reinders, M.E., Leuning, D.G., de Fijter, J.W., Hoogduijn, M.J., and Rabelink, T.J. (2014). Mesenchymal stromal cell therapy for cardio renal disorders. Curr. Pharm. Des. *20*, 2412–2429.

Riazi, A.M., Kwon, S.Y., and Stanford, W.L. (2009). Stem cell sources for regenerative medicine. Methods Mol. Biol. *482*, 55–90.

Song, B., Smink, A.M., Jones, C.V., Callaghan, J.M., Firth, S.D., Bernard, C.A., Laslett, A.L., Kerr, P.G., and Ricardo, S.D. (2012). The directed differentiation of human iPS cells into kidney podocytes. PLoS ONE *7*, e46453.

Souidi, N., Stolk, M., and Seifert, M. (2013). Ischemia-reperfusion injury: beneficial effects of mesenchymal stromal cells. Curr. Opin. Organ Transplant. *18*, 34–43.

Streckfuss-Bömeke, K., Wolf, F., Azizian, A., Stauske, M., Tiburcy, M., Wagner, S., Hübscher, D., Dressel, R., Chen, S., Jende, J., et al. (2013). Comparative study of human-induced pluripotent stem cells derived from bone marrow cells, hair keratinocytes, and skin fibroblasts. Eur. Heart J. *34*, 2618–2629.

Tada, M., Tada, T., Lefebvre, L., Barton, S.C., and Surani, M.A. (1997). Embryonic germ cells induce epigenetic reprogramming of somatic nucleus in hybrid cells. EMBO J. *16*, 6510–6520.

Takahashi, K., and Yamanaka, S. (2006). Induction of pluripotent stem cells from mouse embryonic and adult fibroblast cultures by defined factors. Cell *126*, 663–676.

Takakura, Y., Morita, T., Fujikawa, M., Hayashi, M., Sezaki, H., Hashida, M., and Borchardt, R.T. (1995). Characterization of LLC-PK1 kidney epithelial cells as an in vitro model for studying renal tubular reabsorption of protein drugs. Pharm. Res. *12*, 1968–1972.

Takasato, M., Er, P.X., Becroft, M., Vanslambrouck, J.M., Stanley, E.G., Elefanty, A.G., and Little, M.H. (2014). Directing human embryonic stem cell differentiation towards a renal lineage generates a self-organizing kidney. Nat. Cell Biol. *16*, 118–126.

Thomson, J.A., Itskovitz-Eldor, J., Shapiro, S.S., Waknitz, M.A., Swiergiel, J.J., Marshall, V.S., and Jones, J.M. (1998). Embryonic stem cell lines derived from human blastocysts. Science *282*, 1145–1147.

Tögel, F., Hu, Z., Weiss, K., Isaac, J., Lange, C., and Westenfelder, C. (2005). Administered mesenchymal stem cells protect against ischemic acute renal failure through differentiation-independent mechanisms. Am. J. Physiol. Renal Physiol. *289*, F31–F42.

Unbekandt, M., and Davies, J.A. (2010). Dissociation of embryonic kidneys followed by reaggregation allows the formation of renal tissues. Kidney Int. *77*, 407–416.

Vierbuchen, T., Ostermeier, A., Pang, Z.P., Kokubu, Y., Südhof, T.C., and Wernig, M. (2010). Direct conversion of fibroblasts to functional neurons by defined factors. Nature *463*, 1035–1041.

Xinaris, C., Benedetti, V., Rizzo, P., Abbate, M., Corna, D., Azzollini, N., Conti, S., Unbekandt, M., Davies, J.A., Morigi, M., et al. (2012). In vivo maturation of functional renal organoids formed from embryonic cell suspensions. J. Am. Soc. Nephrol. *23*, 1857–1868.

Zhou, Q., Brown, J., Kanarek, A., Rajagopal, J., and Melton, D.A. (2008). In vivo reprogramming of adult pancreatic exocrine cells to beta-cells. Nature *455*, 627–632.

Stem Cell Reports

Supplemental Information

Direct Reprogramming of Human Bone Marrow Stromal Cells into Functional Renal Cells Using Cell-free Extracts

Evangelia Papadimou, Marina Morigi, Paraskevas Iatropoulos, Christodoulos Xinaris, Susanna Tomasoni, Valentina Benedetti, Lorena Longaretti, Cinzia Rota, Marta Todeschini, Paola Rizzo, Martino Introna, Maria Grazia de Simoni, Giuseppe Remuzzi, Michael S. Goligorsky, and Ariela Benigni

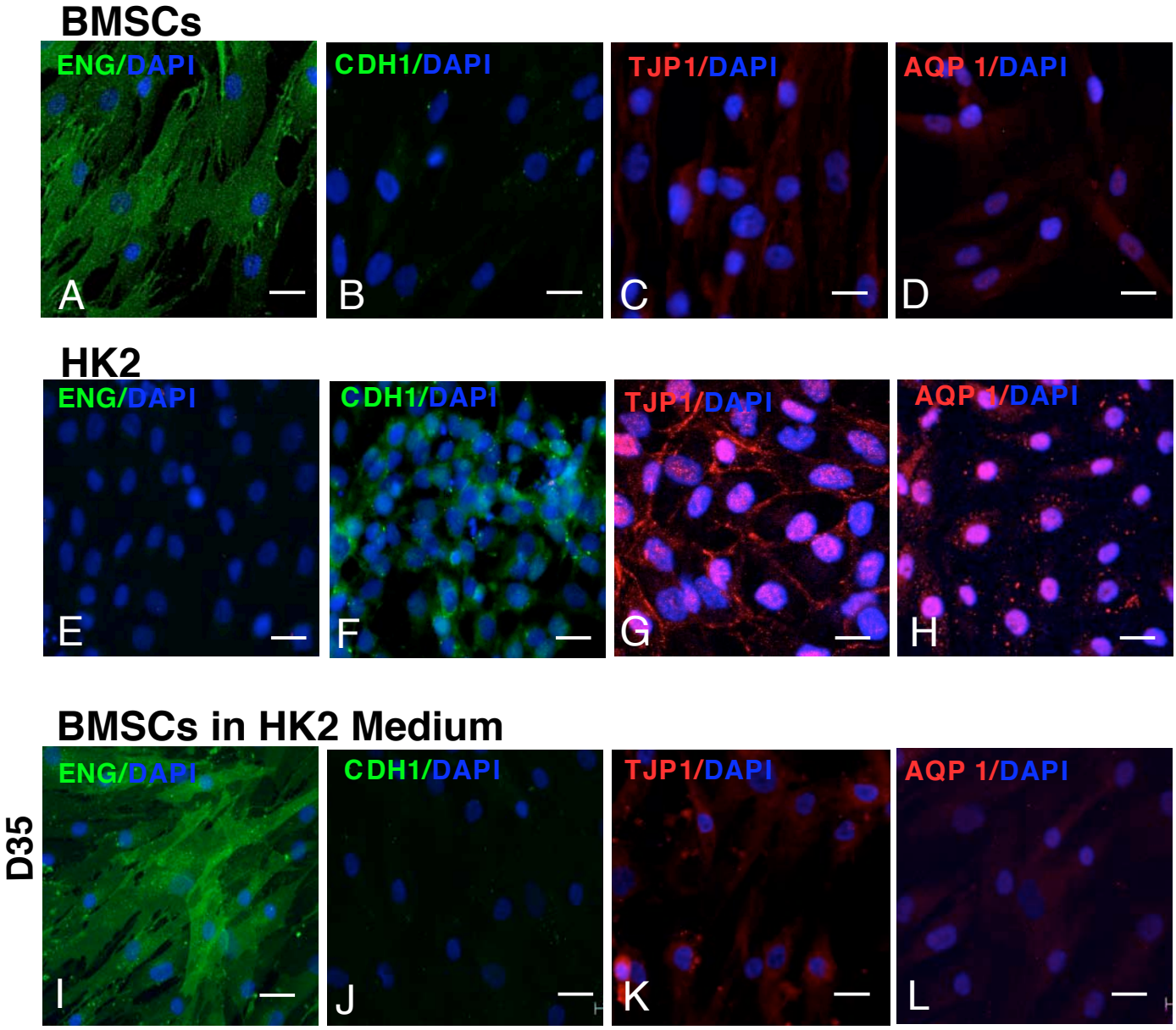
BMSCs
ENG/DAPI
CDH1/DAPI
TJP1/DAPI
AQP 1/DAPI
A
B
C
D
HK2
ENG/DAPI
CDH1/DAPI
TJP1/DAPI
AQP 1/DAPI
E
F
G
H
BMSCs in HK2 Medium
D35
ENG/DAPI
CDH1/DAPI
TJP1/DAPI
AQP 1/DAPI
I
J
K
L

Figure S1

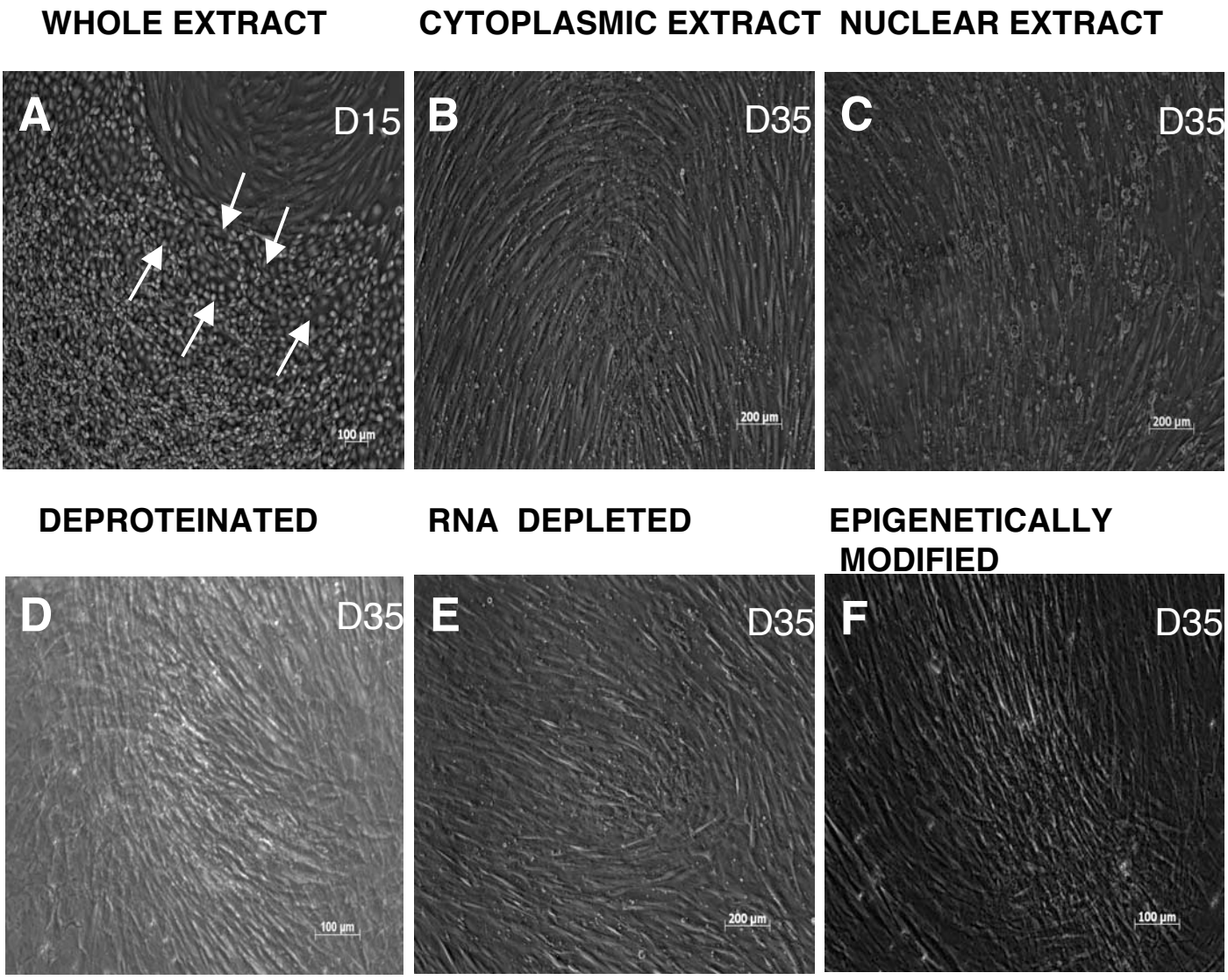
WHOLE EXTRACT
CYTOPLASMIC EXTRACT
NUCLEAR EXTRACT
A
D15
100 µm
B
D35
200 µm
C
D35
200 µm
DEPROTEINATED
RNA DEPLETED
EPIGENETICALLY MODIFIED
D
D35
100 µm
E
D35
200 µm
F
D35
100 µm

Figure S2

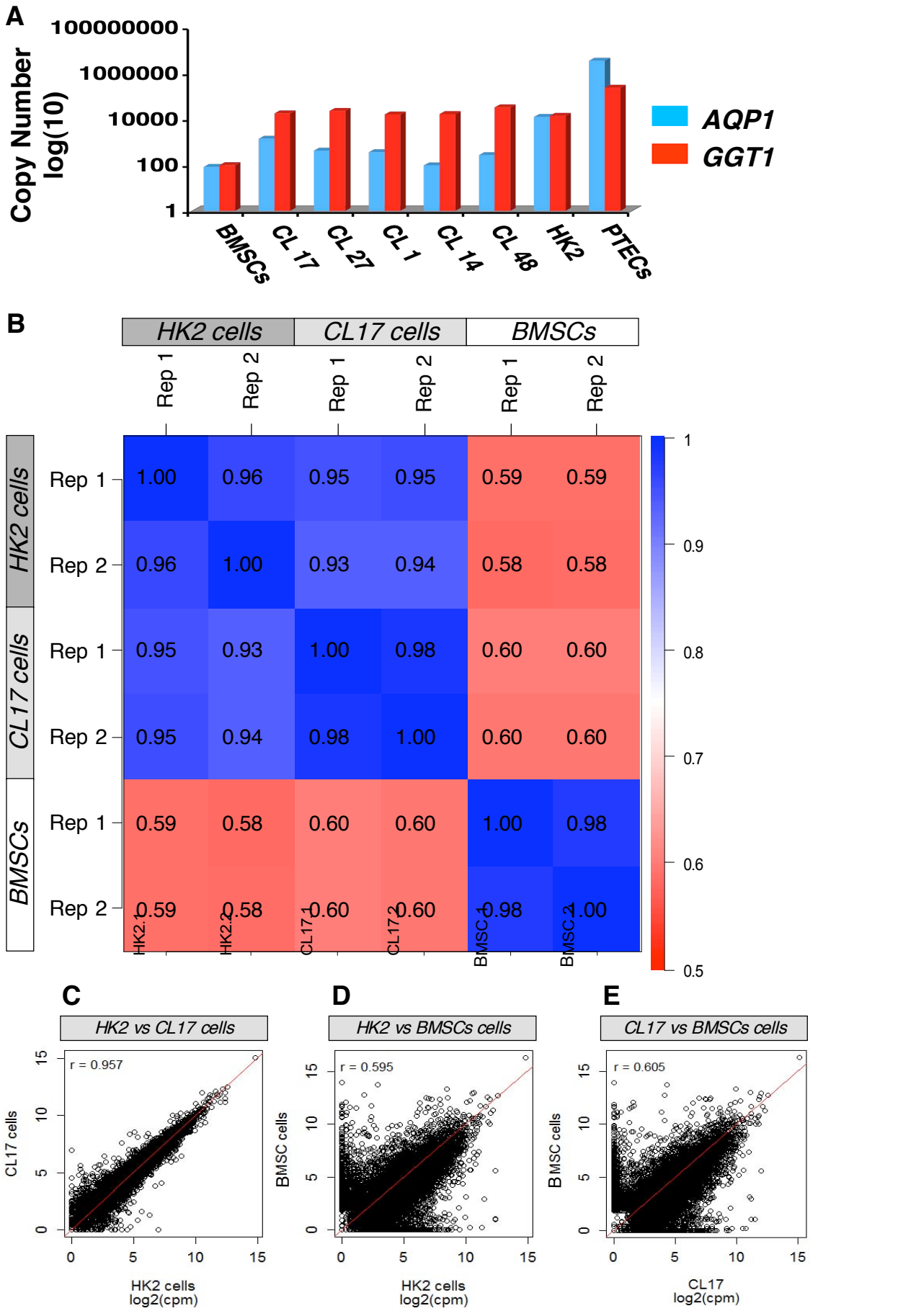
A
Copy Number log(10)
100000000
1000000
10000
100
1
BMSCs
CL 17
CL 27
CL 1
CL 14
CL 48
HK2
PTECs
AQP1
GGT1
B
HK2 cells
CL17 cells
BMSCs
Rep 1
Rep 2
1.00 0.96 0.95 0.95 0.59 0.59
0.96 1.00 0.93 0.94 0.58 0.58
0.95 0.93 1.00 0.98 0.60 0.60
0.95 0.94 0.98 1.00 0.60 0.60
0.59 0.58 0.60 0.60 1.00 0.98
0.59 0.58 0.60 0.60 0.98 1.00
HK2.1
HK2.2
CL17.1
CL17.2
BMSC.1
BMSC.2
1
0.9
0.8
0.7
0.6
0.5
C
HK2 vs CL17 cells
r = 0.957
CL17 cells
HK2 cells log2(cpm)
D
HK2 vs BMSCs cells
r = 0.595
BMSC cells
HK2 cells log2(cpm)
E
CL17 vs BMSCs cells
r = 0.605
BMSC cells
CL17 log2(cpm)

Figure S3

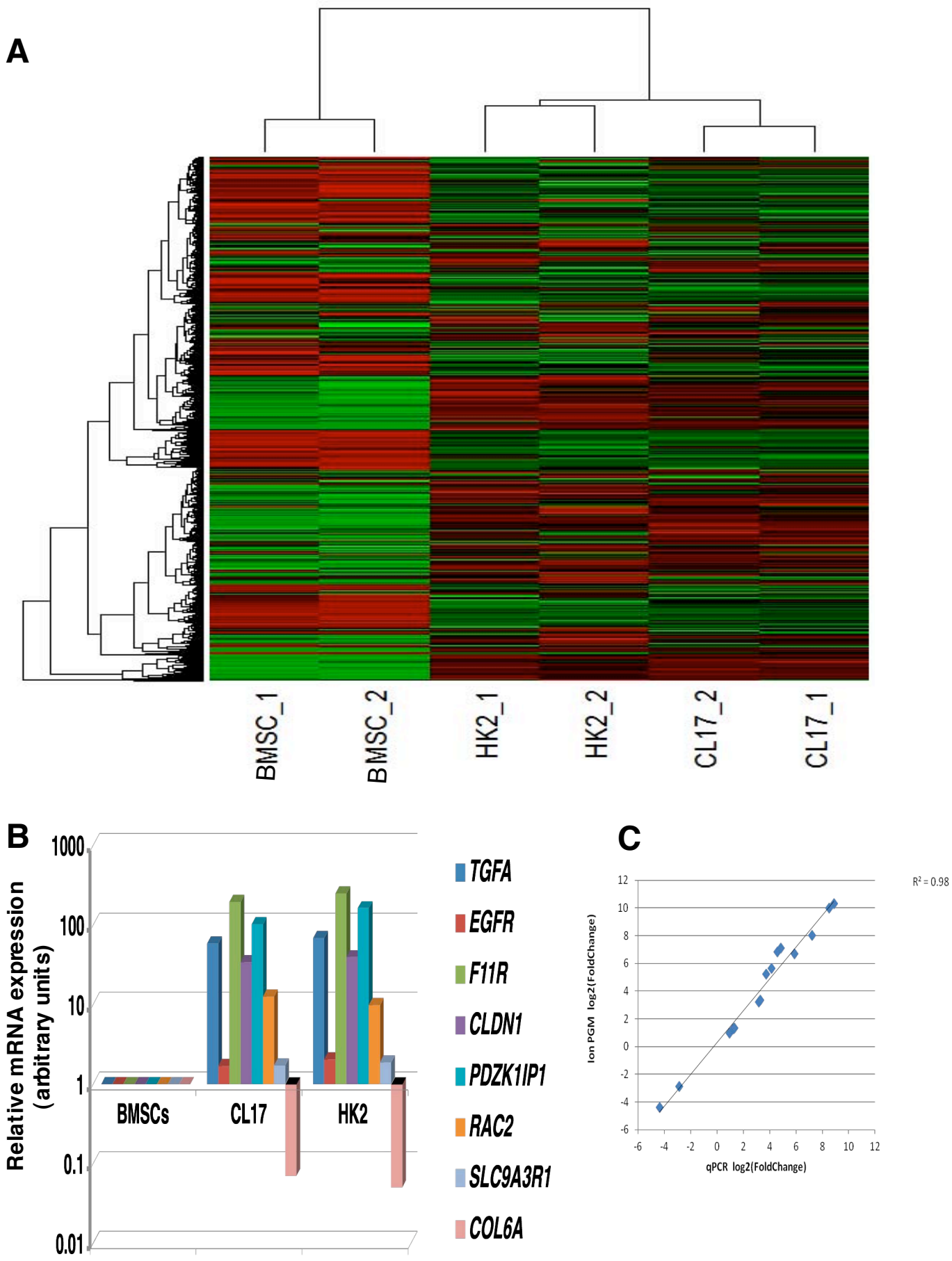
A
BMSC_1
BMSC_2
HK2_1
HK2_2
CL17_2
CL17_1
B
Relative mRNA expression (arbitrary units)
1000
100
10
1
0.1
0.01
BMSCs
CL17
HK2
TGFA
EGFR
F11R
CLDN1
PDZK1IP1
RAC2
SLC9A3R1
COL6A
C
R² = 0.98
Ion PGM log2(FoldChange)
qPCR log2(FoldChange)
12
10
8
6
4
2
0
-2
-4
-6
-6
-4
-2
0
2
4
6
8
10
12

Figure S4

EGFR – Tight Junction

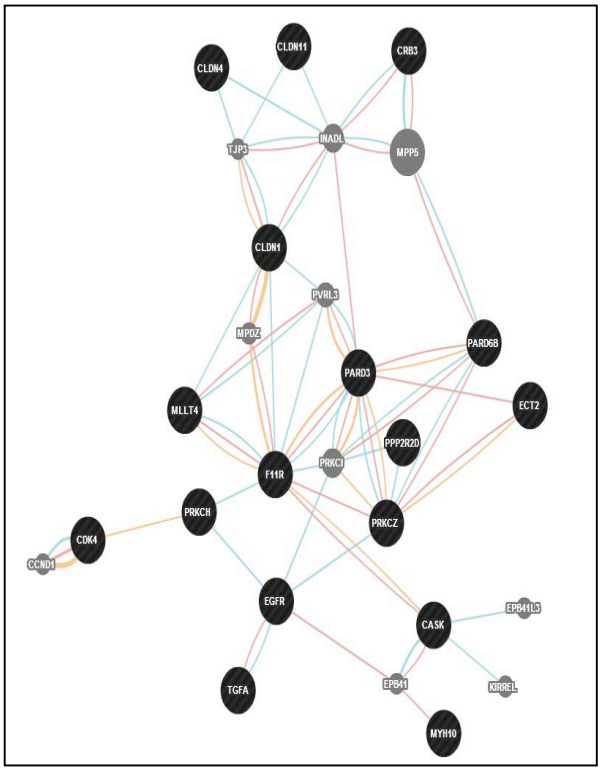

EGFR –Focal adhesion

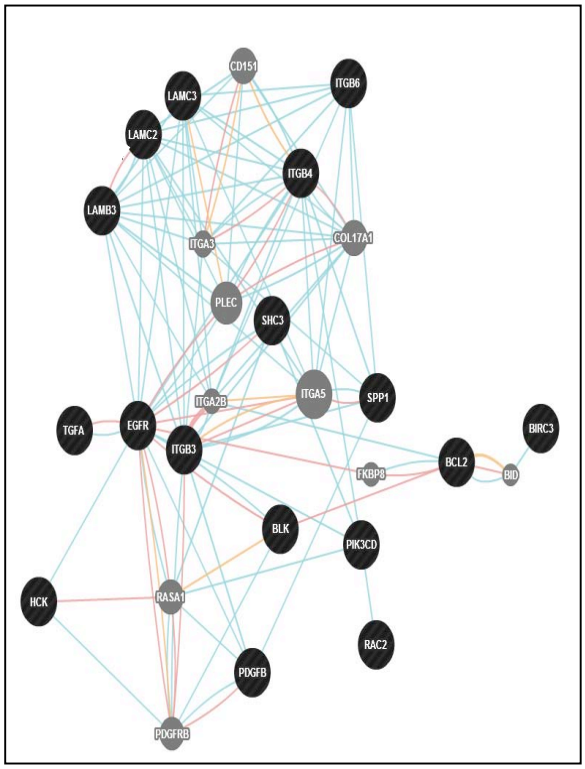

EGFR – Brush border

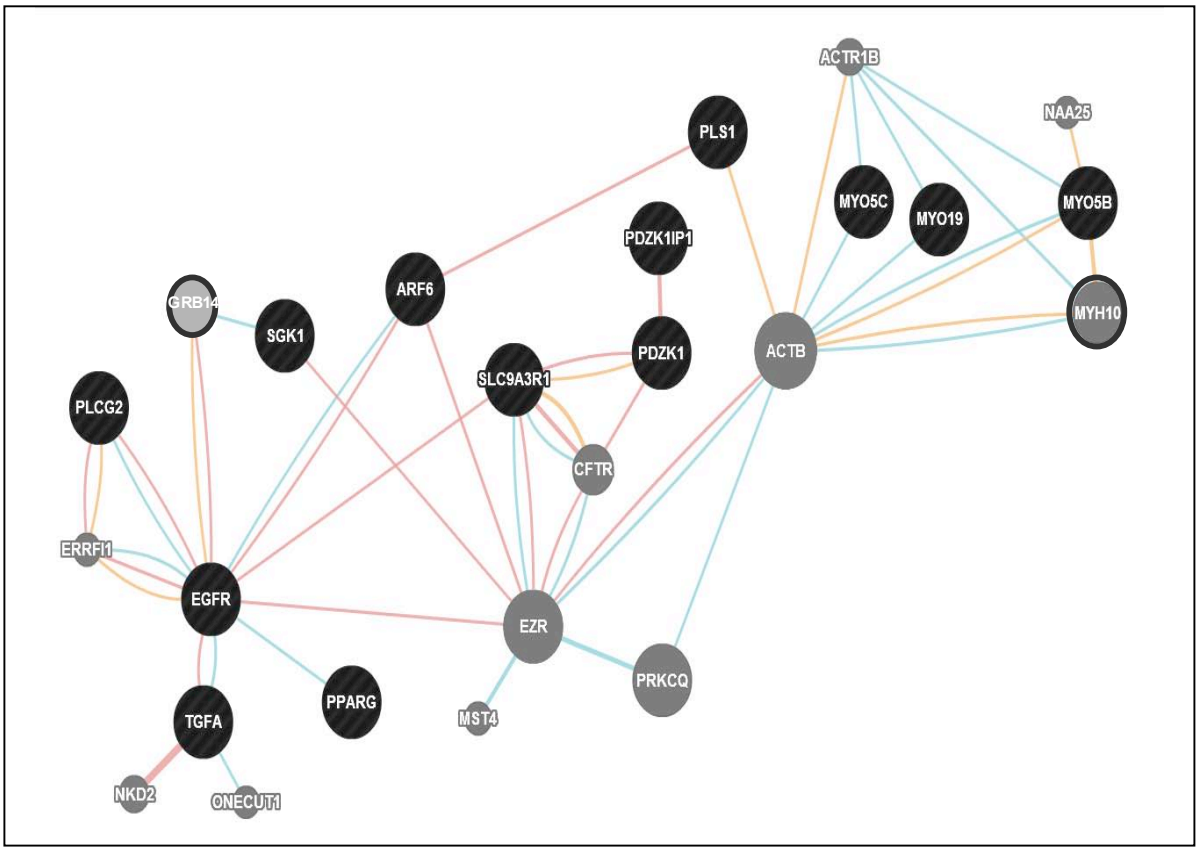

Figure S5

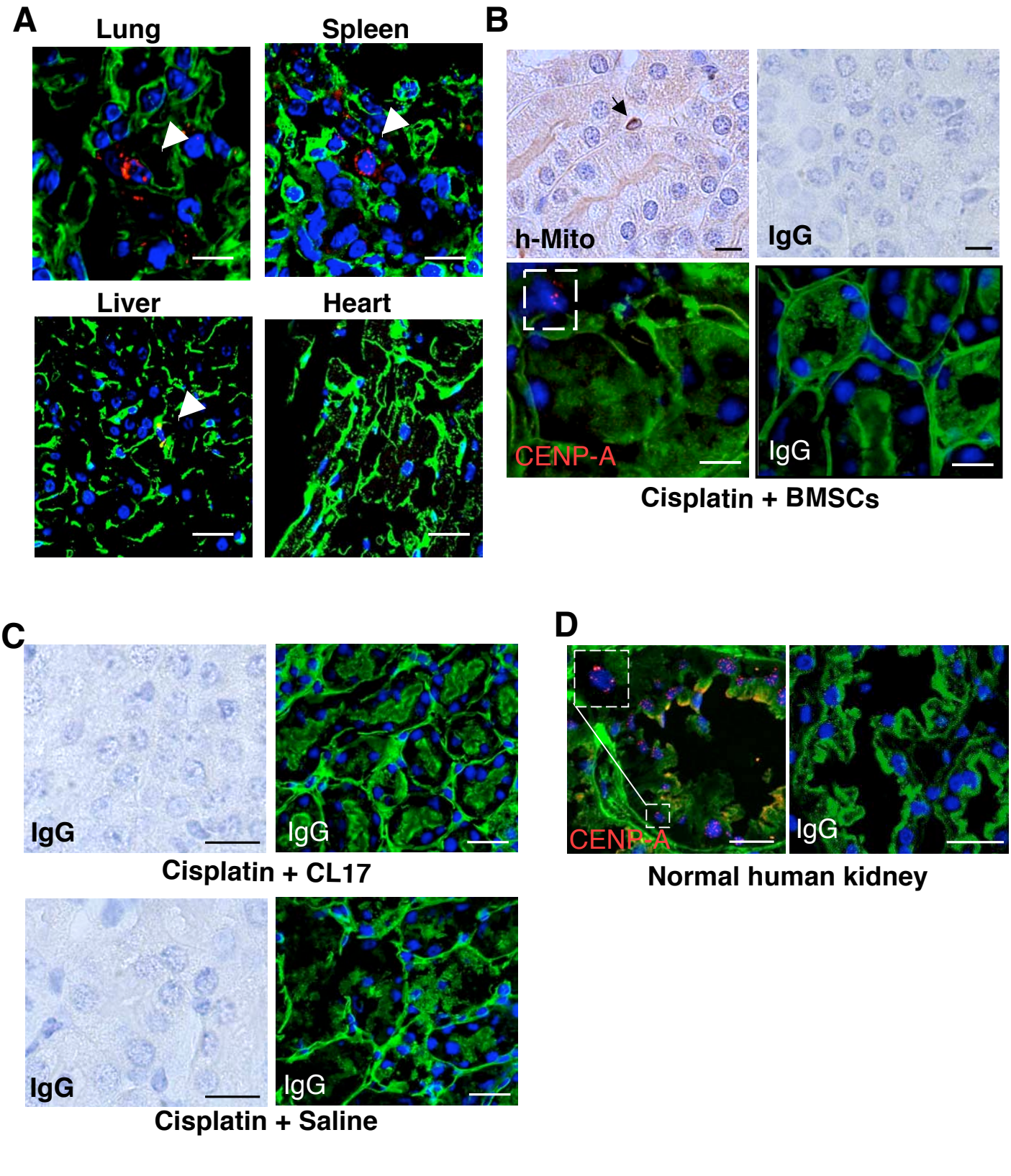
A
Lung
Spleen
Liver
Heart
B
h-Mito
IgG
CENP-A
IgG
Cisplatin + BMSCs
C
IgG
IgG
Cisplatin + CL17
IgG
IgG
Cisplatin + Saline
D
CENP-A
IgG
Normal human kidney

Figure S6

SUPPLEMENTAL FIGURE LEGENDS

Figure S1, Related to Figure 2: Antigenic profile of BMSCs, HK2 cells and BMSCs in HK2 medium.

Expression of ENG, CDH1, TJP1 and AQP1 in BMSCs **(A-D)** HK2 cells **(E-H)** and in BMSCs grown in HK2 specific media for 35 days **(I-L)**. Scale bar: 50μm. Images are representative of two independent experiments.

Figure S2: Reprogramming of BMSCs with modified extracts.

BMSC treated with whole extract changed their spindle like shape into cobble stone colonies at day 15 (**A,** arrows). When BMSCs were treated with cytoplasmic or nuclear extract alone no cell change occurred after 35 days **(B-C)**. Deproteinated or RNA depleted extract did not produce any change at 35 days **(D-E)**. Treatment of HK2 extracts with the epigenetic modifiers Trichostatin A and 5-aza-cytidine did not lead to any cell type change in BMSC at 35 days post-treatment **(F)**. Images are representative of two independent experiments for each condition.

Figure S3, Related to Figure 3A and 3E

(A) Absolute quantification of *AQP1* and *GGT1* mRNA by qRT-PCR in BMSCs, in 5 selected clones, in HK2 cells and in primary PTECs.

(B) Pearson correlation coefficients among all analyzed samples. The higher and the lower coefficients are coloured in a blue to red gradient. **(C-E)** Scatter plots representing the expression of each gene in the indicated pairs of cell types and Pearson correlation coefficients among samples.

Figure S4, Related to Figure 3G

(A) Heatmap of all the genes with ≥5 reads in at least one replicate of each cell lineage. Columns represent biological replicates, and rows represent genes. Green and red colours indicate high and low expression, respectively. The dendrogram of the unsupervised hierarchical clustering of the analyzed samples is shown in the upper part of the heatmap. **(B)** Relative expression of mRNA of human *TGFA, EGFR, F11R, CLDN1, PDZK1 IP1, RAC2, SLC9A3R1, COL6A* by qRT-PCR in CL17 and HK2 in comparison to BMSCs. BMSC mRNA expression was used as the reference sample. The qRT-PCR of these markers, involved in pathways of the BMSC reprogramming, confirmed the fold inductions observed by RNA-seq validating the approach. (C) Comparison between qPCR and Ion PGM data revealed a very high concordance with an R-squared correlation coefficient of 0.98.

Figure S5, Related to Figure 3G

EGFR pathway upregulation and its correlation with genes involved in tight junction, focal adhesion and brush border networks in the reprogrammed BMSCs. Black filled circles represent up-regulated genes of the specific pathway emerged from the functional network analysis with ToppFun and GraphiteWeb. In each pathway 10 genes have been added by GeneMania software to complete the network (filled grey circles). Some of the genes added by GeneMania are up-regulated in CL17 cells (filled grey bold circles). Pink lines represent known physical interactions, blue lines indicate that they belong to same pathway, and yellow lines that are predicted to belong to the same pathway.

Figure S6, Related to Figure 6

(A) Detection of $PKH26^{+ve}$ CL17 cells in different organs than the kidney of AKI mice at day 4. Representative images of $PKH26^{+ve}$ CL17 cells in the lung, spleen, liver (arrowheads), and heart. Scale bars: upper panels 10μm; lower panels: 20 μm. (B) Representative pictures

for h-Mito (upper left panel) and CENP-A staining (bottom left panel) and the respective negative controls (right panels) in renal tissue of mice with cisplatin-induced AKI receiving control BMSCs. Scale bars: 10 μm. Nuclei were stained with DAPI (blue) and renal structures were labelled with wheat germ agglutinin (WGA, green). (C) Representative pictures showing negative controls for h-Mito (left panels) and CENP-A staining (right panels) in AKI animals receiving CL17 (upper panels) or saline (bottom panels). Scale bars: 10 μm for h-Mito and 20 μm for CENP-A staining. (D) Representative pictures showing CENP-A staining in normal human kidney used as positive sample (left panel) and the respective negative control (right panel). Scale bars: 20 μm.

SUPPLEMENTAL TABLES

Table S1. Top 20 down-regulated genes (min fold change) in CL17 vs BMSCs.

Gene	logFC	Fold change	p-adjusted	Down-regulated in HK2 vs BMSCs
COL1A2	-18.5	376095	3.5E-43	Yes
MMP2	-16.4	87057	1.6E-181	Yes
COL6A3	-16.3	78144	8.9E-108	Yes
SULF1	-16.2	74199	1.4E-178	Yes
COL3A1	-15.6	51079	5.2E-24	Yes
TIMP3	-15.5	45853	2.1E-158	Yes
ACAN	-15.3	39800	3.5E-19	Yes
POSTN	-15.2	37533	3.4E-27	Yes
ITGBL1	-14.5	22743	2.3E-132	Yes
CXCL12	-14.4	21579	1.9E-109	Yes

ADAMTS2	-14.2	19048	1.8E-125	Yes
CDH11	-14.2	18687	1.6E-124	Yes
PENK	-14.1	17999	1.7E-09	Yes
CD248	-13.8	14240	1.4E-113	Yes
ITGA11	-13.7	13259	4.0E-14	Yes
HSPB7	-13.5	11573	4.0E-104	Yes
COL5A1	-13.3	10432	6.7E-36	Yes
BGN	-13.2	9284	8.7E-21	Yes
SCUBE3	-13.2	9169	1.3E-50	Yes
LAMA4	-13.0	8024	1.8E-48	Yes

Table S2. Top 20 up-regulated genes (max fold change) in CL17 vs BMSCs.

Gene	**logFC**	**Fold change**	**p-adjusted**	**Up-regulated in HK2 vs BMSCs**
CXCL5	13.4	10840	2.8E-58	Yes
SERPINA1	13.2	9600	3.8E-36	Yes
LCN2	12.4	5340	1.2E-05	Yes
GNG4	12.3	4964	6.0E-60	Yes
CLEC4E	12.2	4796	1.6E-07	Yes
IGFN1	12.1	4368	2.4E-43	Yes
ELF3	11.9	3821	1.9E-31	Yes
HKDC1	11.9	3798	4.4E-37	Yes
EEF1A2	11.9	3713	3.0E-110	Yes
GALNT14	11.7	3427	2.2E-32	Yes

TM4SF18	11.7	3420	8.4E-39	Yes
ARHGAP40	11.7	3293	1.1E-48	Yes
HNF1B	11.6	3089	1.5E-48	Yes
CSF2	11.5	2894	8.8E-27	Yes
SLCO4A1	11.5	2833	1.9E-48	Yes
DCDC2	11.3	2459	6.3E-42	Yes
F11R	11.3	2445	1.5E-41	Yes
COCH	11.2	2407	1.6E-41	Yes
SLCO2A1	11.2	2346	7.2E-09	Yes
LRRN4	11.1	2270	2.2E-41	Yes

Table S3. Functional characterization DEG for selected pathways.xls

SUPPLEMENTAL EXPERIMENTAL PROCEDURES

Transmission Electron microscopy

Human BMSCs, clone 17 (CL17), and HK2 cells grown on thermanox slides (Nunc), were fixed for 4 hours in 2.5% glutaraldehyde in 0.1 M cacodylate buffer, pH 7.4, and washed repeatedly in the same buffer. After postfixation in 1% OsO4, specimens were dehydrated through ascending grades of alcohol and embedded in Epon resin (Fluka, Sigma-Aldrich). Ultra thin sections were stained with uranyl acetate and lead citrate and examined by using transmission electron microscope (Morgagni 268D, Brno, Czech Republic).

Scanning electron microscopy

For scanning electron microscopy (SEM) analysis, BMSCs, HK2 and CL17 cells, seeded on thermanox slides, were fixed in 2.5% glutaraldehyde (buffered with 0.1 M sodium cacodylate buffer, pH 7.4) for 1 hour, postfixed in 1% osmium tetroxide and dehydrated

through an increasing ethanol series. Cell monolayers were then dried with pure hexamethyldisilazane (HMDS, Fluka Chemie AG, Buchs, Switzerland) (twice for 30 minutes), sputter-coated with gold and observed at SEM (Supra 55, Zeiss, Oberkochen, Germany).

Immunocytochemistry

Immunocytochemistry was performed following standard procedures. Primary antibodies to CD105 (1:100, Dako, catalogue n (cat. n): M3527), CDH1 (1:50, Beckton Dickinson, cat. n: 610182), TJP1 (1:50, cat. n: sc-10804), AQP1 (1:50, cat. n: sc-20810) and GGT1 (1:25, cat. n: sc-20638) from Santa Cruz, were incubated overnight at 4^{o}C. Secondary antibodies (1:50, anti-IgG FITC and 1:50 anti-IgG Cy3 Jackson Laboratories) were incubated for 1 hour at room temperature. 4',6-Diamidino-2-Phenylindole, Dihydrochloride (DAPI) (1:10000, Molecular Probes) was used to visualise the nuclei. Cells were mounted (Dako mounting solution) and fluorescent images were acquired using an Apotome microscope, Axion Vision, Imager 2Z, Zeiss

Flow cytometry

Flow cytometry analysis was performed following standard procedures using a FACSAria (BD) machine. The following conjugated antibodies were used: ENG-PE (Caltag, Invitrogen, cat. n: MHCD10504), CDH1-Alexa-488 (Cell Signaling, Invitrogen, cat. n: 31995), Aquaporin 1-Fluorescein Isothyocyanate (AQP1-FITC) (Santa Cruz, cat. n: sc-32737 FITC) or isotype-matched control antibodies.

Generation of Clones using limiting dilution

Human BMSC treated with HK2 extracts were used for limiting dilution at first passage to

generate clones. Cells were dissociated with trypsin-EDTA and plated into single cell suspension into four 96-well plates (BD) in HK2 medium. Wells containing more than one cell were excluded from the study. When the 96 wells were confluent the clones were subcultured in higher dimension plates/flasks sequentially. Fifty clones (out of total 240 individual cells inoculated) were isolated and expanded. One half of each of fifty clones was frozen at liquid N2 and the other half was collected into Trizol (Ambion, Invitrogen) and kept at -20^{o}C until further analysis. Clones were generated from one reprogramming experiment using one human BMSC donor.

Duplication time measurement

Duplication time was evaluated as previously described (Korzynska and Zychowicz, 2008). Human BMSCs, CL17 and HK2 cells were plated at the density of 30,000 cells/well (n=5), and the number of cells was counted at different time intervals. Growth curves were produced for each cell line and the duplication time was calculated at the linear part of the curve between time intervals of 24-48 hours for HK2 and CL17 cells and 7-14 days for BMSCs. The equation $T2=\Delta t/\log_2(\Delta N/N_0+1)$ was used for the calculation of the duplication time. In this equation N_0 is the number of cells at the beginning of observation (seeding density) and ΔN is the increase in the number of cells during the period of time of the length Δt (Korzynska and Zychowicz, 2008).

RNA extraction, qRT-PCR

Total RNA was prepared from BMSCs, HK2 cells and five of the clones obtained by limiting dilution, using TRIzol reagent according to the manufacturer's instructions. Contaminating genomic DNA was removed by RNase-free DNase (Promega) for 1h at 37°C. Two μg of purified RNA was reverse transcribed using a mixture of oligodT and random

examers oligonucleotides and 200U of SuperScript II RT (Invitrogen) for 1h at 42°C. No enzyme was added for reverse transcriptase-negative controls.

To amplify human cDNAs, we used SYBR Green PCR Master Mix (Applied Biosystems) according to the manufacturer's instruction. qRT-PCR was performed on a 7300 Real Time PCR System (Applied Biosystems). The amplification profile consisted of 2 min at 50°C and 10 min at 95°C, the samples were cycled 40 times at 95°C for 15 s and 60°C for 60 s. We used the ΔΔCt technique to calculate cDNA content in each sample using the cDNA expression in BMSCs or HK2 cells as calibrator.

For absolute quantification of the copy number of human *AQP1* and human *GGT1* transcripts, commercially synthesized oligonucleotides (450 bp) were obtained (Sigma-Aldrich). The DNA was serially diluted (40, $4x10^2$, $4x10^3$, $4x10^4$, $4x10^5$ and $4x10^6$ copies) to make a standard curve (Bustin, 2000).

From the standard series included in the PCR, a linear relationship between Ct and log10 (DNA copy number) was plotted for a target transcript. Based on the relationship, the *C*t value for a given sample was used to infer its corresponding amount of template. Because the target gene sequence was known, it was possible to calculate the copy numbers by the molecular weight of the sequence, which estimated the copy number in an unknown sample (Wang et al., 2014).

The primers that were used are listed following:

Gene	***Sequences***
RPL29	For 5'-AGCCCCTTTCTCTTCCGGTT-'3
(NM_000992.2)	Rev 5'-GTGCCATTTTCGGGACTGGT-'3
AQP1	For 5'-CCCTCATGTACATCATCGCCC-'3
(NM_198098.2)	Rev 5'-ACACCATCAGCCAGGTCATT-'3
GGT1	For 5'-AGCCTGTCTTGTGTGAGGTG-'3
(NM_001032364.2)	Rev 5'-TGAGGCTGCCGTTGTAGAAG-'3
ENG	For 5'-AGCCCTGACCTGTCTGGTTG-'3
(NM_001114753.1)	Rev 5'-GAACGCGTGTGCGAGTAGA-'3

TGFa	For 5'-TCCCCGCTGAGTGACCC-'3
(NM_001099691.2)	Rev 5'-CTCCTGCACCAAAAACCTGC-'3
EGF-R	For 5'-GAGCAGCGATGCGACCCT-'3
(NM_005228.3)	Rev 5'-CTTGGCAAACTTTCTTTTCCTCCA-'3
F11R	For 5'-GGCTTTTCTTCTCCCCGTGT-'3
(NM_016946.4)	Rev 5'-CCGGTCCTCATAGGAAGCTGT-'3
CLDN1	For 5'-CAGTCAATGCCAGGTACGAA-'3
(NM_021101.4)	Rev 5'-ACAGCAAAGTAGGGCACCTC-'3
PDZK1IP1	For 5'-CGTCGGAAACAAGGCAGATG-'3
(NM_005764.3)	Rev 5'-CATGCTCACTGGACCTGAAAC-'3
RAC2	For 5'-TCACCACCGACACTCTCCAG-'3
(NM_002872.4)	Rev 5'-CCACGGCCCCATCTCCC-'3
SLC9A3-R1	For 5'-CGAGGAGCTGAATTCCCAAGA-'3
(NM_004252.4)	Rev 5'-AGTCTAGGATGGGGTCGGAG-'3
COL6A2	For 5'-ATGACGCTGTTCTCCGACCT-'3
(NM_001849.3)	Rev 5'-ACGGACAGCTCTGTTTGGCA-'3

Albumin binding and uptake assay

Albumin binding and uptake assays were performed as previously described (Gekle et al 1998, Morigi et al., 2005) with small modifications. Human BMSCs, CL17 and HK2 cells were incubated with serum free medium over night. Cells were washed 3x with Ringer's buffer pH 6.0 and then were exposed to 50μg/ml BSA-FITC (Bovine Serum Albumin, Sigma-Aldrich) alone or in the precence of an excess of unlabeled BSA (5mg/ml) for 15 min at 4^{o}C for binding studies and for 90 min at 37^{o}C for uptake experiments. The cells were then washed 3x with Ringer's buffer pH 7.4, fixed in 2% PFA and 4% sucrose for 10 min at RT. Cells were mounted with mounting solution and images were acquired using an Apotome microscope, Axion Vision, Imager 2Z, Zeiss.

Renal organoids

Briefly, E11.5 CD1 mouse embryonic kidneys were dissected in MEM (Sigma-Aldrich) placed in 1x trypsin/EDTA (Biochrom AG) for 3 min at 37°C and then dissociated by trituration into single-cell suspensions that were filtered through a 40-μm cell strainer

(Falcon, BD). Human cells were labeled with Cell Tracker (Molecular Probes) following the manufacturer's instructions and labelling efficacy and viability were evaluated by Trypan blue (Sigma-Aldrich) exclusion. A total of $1x10^5$ freshly dissociated renal cells were centrifuged at 900 g for 4 min in the presence of $1x10^4$ CL17, HK2 or BMSCS then the pellet was placed on a top of a 5 μm filter (Millipore) supported by a metal grid, at the air–medium interface in a humidified atmosphere with 5% CO_2 and at 37°C and maintained in Advanced DMEM supplemented with 2% Embryonic Stem cells Fetal Bovine Serum, 1% L-glutamine and 1% penicillin/streptomycin (all from Gibco, Invitrogen). During the first 24 h, aggregates were cultured in the presence of 1.25 μmol/l Glycyl-H1152 dihydrochloride (Tocris), a Rho kinase inhibitor. Renal chimeras were cultured *in vitro* for 1 or 5 days, then fixed and finally processed for immunofluorescence analysis, as previously described (Xinaris et al., 2012).

Renal histology and Immunohistochemistry Analysis

Duboscq-Brazil fixed, paraffin embedded kidney samples were stained with periodic acid–Schiff's reagent (PAS) and observed by light microscopy (Primo Star, Zeiss, Jena, Germany). Luminal hyaline casts and tubular necrosis (denudation of tubular basement membrane) were assessed in up to 25 non overlapping fields/section for each animal (40x, high power field, HPF).

For immunofluorescence staining, acetone-fixed cryosections were subjected to antigen retrieval using microwave (twice for 5 min in citrate buffer 10mM pH 6.0 at operating frequency of 2450 MHz and 600W power output). After blocking with 1% BSA, sections were incubated with rabbit anti-human CENP-A (Cell Signalling Technology, Danvers, MA, USA, dilution 1:100; cat. n: 2186) followed by goat anti-rabbit Cy3-conjugated secondary antibody (Jackson ImmunoResearch Laboratories, West Grove, PA). Cell nuclei were

labelled with DAPI and renal structures with fluorescein wheat germ agglutinin (WGA, VECTOR Labotatories, cat. n: FL-1021). Human tissue was used as positive control (Figure S 6D). Fluorescence was examined using an inverted confocal laser-scanning microscope (LSM 510 Meta).

For immunoperoxidase experiments, Duboscq-Brazil fixed, paraffin embedded renal sections (3μm) were deparaffinised, hydrated and incubated for 5 min with Peroxidased1 solution (Biocare, Concord, CA) to quench endogenous peroxidases. Antigen retrieval was performed by boiling sections using microwave in Rodent Decloacker solution. After blocking with Rodent Block M (Biocare), sections were incubated with anti-human mitochondria (Millipore, Temecula, CA, USA, dilution 1:50; cat. n: mab1273) followed by specific mouse-on-mouse polymer kit (Biocare) and diaminobenzidine (Merck, Darmstadt, Germany) substrate solution. Slides were finally counterstained with hematoxylin, dehydrated in graded alcohols, mounted with coverslips, and observed by light microscopy (Apotome Axio Imager Z2, Zeiss, Jena, Germany). Negative controls for immunofluorescence and immunoperoxidase experiments were obtained by incubating the adjacent section of examined renal tissue with non-immune immunoglobulin of the same isotype of the primary antibody.

SUPPLEMENTAL REFERENCES

Bustin, S.A. (2000). Absolute quantification of mRNA using real-time reverse transcription polymerase chain reaction assays. J Mol Endocrinol *25*, 169-193.

Korzynska, A., and Zychowicz, M. (2008). A method of estimation of the cell doubling time on basis of the cell culture monitoring data. Biocybernetics and Biomedical Engineering *28*, 75-82.

Wang, Y., Fan, Q., Ma, R., Lin, W., and Tang, T. (2014). Gene expression profiles and phosphorylation patterns of AMP-activated protein kinase subunits in various mesenchymal cell types. Chin Med J (Engl) *127*, 2451-2457.